

National Bureau of Standards  
Library, E-01 Admin. Bldg.

Copy 2

FEB 17 1971

# NBS TECHNICAL NOTE 541

ED STATES  
TMENT OF  
MERCER  
ICATION



## Preliminary Study on the Characteristics and Design Parameters for a Mössbauer Resonant Detector

U.S.  
ARTMENT  
OF  
MMERCE  
National  
Bureau  
of  
Standards



410  
100  
753  
571  
1

UNITED STATES DEPARTMENT OF COMMERCE

Maurice H. Stans, Secretary

U.S., NATIONAL BUREAU OF STANDARDS • Lewis M. Branscomb, Director



TECHNICAL NOTE 541

ISSUED JANUARY 1971

Nat. Bur. Stand. (U.S.), Tech. Note 541, 65 pages (Jan. 1971)

CODEN: NBTNA

**Preliminary Study on the Characteristics  
and Design Parameters for a Mössbauer  
Resonant Detector**

J. J. Spijkerman, J. C. Travis,  
P. A. Pella, and J. R. DeVoe

Radiochemical Analysis Section  
Analytical Chemistry Division  
Institute for Materials Research  
National Bureau of Standards  
Washington, D.C. 20234



NBS Technical Notes are designed to supplement the Bureau's regular publications program. They provide a means for making available scientific data that are of transient or limited interest. Technical Notes may be listed or referred to in the open literature.



## FOREWORD

The Analytical Chemistry Division was established as a separate division at the National Bureau of Standards on September 1, 1963, and became part of the Institute for Materials Research in the February 1, 1964, reorganization. It consists at present of nine sections and about 100 technical personnel encompassing some 60 different analytical competences from activation analysis and atomic absorption to vacuum fusion and x-ray spectroscopy. These competences, and in turn the sections which they comprise, are charged with research at the forefront of analysis as well as awareness of the practical sample, be it standard reference material or service analysis. In addition it is their responsibility to inform others of their efforts.

Formal publication in scientific periodicals is a highly important output of our laboratories. In addition, however, it has been our experience that informal, annual summaries of progress describing efforts of the past year can be very valuable in disseminating information about our programs. A word is perhaps in order about the philosophy of these yearly progress reports. In any research program a large amount of information is obtained and techniques developed which never find their way into the literature. This includes the "negative results" which are so disappointing and unspectacular but which can often save others considerable work. Of importance also are the numerous small items which are often explored in a few days and which are not important enough to warrant publication--yet can be of great interest and use to specialists in a given area. Finally there are the experimental techniques and procedures, the designs and modifications of equipment, etc., which often require months to perfect and yet all too often must be covered in only a line or two of a journal article.

Thus our progress reports endeavor to present this information which we have struggled to obtain and which we feel might be of some help to others. Certain areas which it appears will not be treated fully in regular publications are considered in some detail here. Other results which are being written up for publication in the journal literature are covered in a much more abbreviated form.

At the National Bureau of Standards publications such as these fit logically into the category of a Technical Note. In 1970 we plan to issue these summaries for all of our sections. The following is the seventh annual report on progress of the Radiochemical Analysis Section.

W. Wayne Meinke, Chief  
Analytical Chemistry Division

## PREFACE

This progress report serves the dual purpose of providing the status of a very important project involving detector design for Mössbauer spectroscopy and the progress of the Radiochemical Analysis Section for the year. Indeed as a result of cutbacks during the past eighteen months, the total effort of the section has centered around this work and that of the certification of Standard Reference Materials for Mössbauer spectroscopy. A report on the Standards will be forthcoming.

Significant reorientation of the activities of this section is imminent, and the section's new direction will be reported next year.

This study has been supported in part by the Division of Isotope Development. U. S. Atomic Energy Commission, Washington, D. C. under contract AT-49-2-1165.

James R. DeVoe, Chief  
Radiochemical Analysis Section





# TABLE OF CONTENTS

|  | <u>PAGE</u> |
|--|-------------|
| 1. INTRODUCTION . . . . .  | 1           |
| 2. DETECTION METHODS FOR MÖSSBAUER SPECTROSCOPY . . . . .  | 6           |
| A. Conventional Transmission Method . . . . .  | 6           |
| B. Conventional Scattering . . . . .   | 6           |
| C. Scattering with Detection of Conversion X-Rays . . . . .  | 8           |
| D. Scattering with Detection of Conversion Electrons . . . . .   | 10          |
| E. Transmission Using a Resonant Detector . . . . .  | 13          |
| F. Scattering Using a Resonant Detector . . . . .  | 13          |
| 3. THEORY . . . . .  | 14          |
| A. Internal Conversion Electrons . . . . .   | 14          |
| B. Cross Sections . . . . .  | 14          |
| C. Efficiency . . . . .  | 18          |
| D. Signal-to-background Ratio . . . . .  | 28          |
| E. Line Width . . . . .  | 33          |
| 4. PRELIMINARY MEASUREMENTS . . . . .  | 36          |
| A. Resonant Detector for <sup>119</sup> Sn Using the Gel Scintillation Technique . . . . .   | 36          |
| B. Resonant Detector for <sup>57</sup> Fe Using a Conversion Electron Proportional Counter . . . . .                                 | 40          |
| 5. SUMMARY . . . . .   | 50          |
| 6. REFERENCES . . . . .  | 51          |
| APPENDIX A: TO COMPUTE RESONANT DETECTOR EFFICIENCY AND SIGNAL BACKGROUND RATIO AS A FUNCTION OF ASSORTED INPUT PARAMETERS . . . . . | 53          |
| APPENDIX B: TRIPLE CONVOLUTION OF SOURCE, ABSORBER AND DETECTOR LORENTZIAN PROFILES . . . . .  | 55          |

## LIST OF FIGURES

### FIGURE NO.

|  |   |
|--|---|
| 1. Energy resolution of the various types of processes associated with the 14.4 keV gamma radiation of cobalt-57 . . . . . | 2 |
|--|---|

|     |   |    |
|-----|---|----|
| 2.  | a) Schematic of internal conversion process for the 14.4 keV transition of $^{57}\text{Co}$ . b) Energy degradation process for a source, absorber and detector system in a conventional Mössbauer detection system . . . . .   | 4  |
| 3.  | Detection methods for Mössbauer spectroscopy. a) Conventional transmission. b) Conventional scattering. c) Conversion x-ray scattering. d) Conversion electron scattering. e) Transmission, using a resonant detector. f) Scattering, using a resonant detector . . . . . | 7  |
| 4.  | Attenuation coefficient for 14.4 keV gamma radiation as a function of element [19] . . . . .  | 9  |
| 5.  | Number of 6.3 keV internal conversion x-rays from Fe as a function of the penetration into the sample for backscattering geometry . . . . .   | 10 |
| 6.  | X-ray detection Mössbauer scattering spectra for iron foil on stainless steel foil . . . . .  | 11 |
| 7.  | Conversion-electron detection Mössbauer back-scattering spectra for vacuum-deposited iron on stainless steel foil . . . . .   | 12 |
| 8.  | Transmission of parallel electrons through $\text{FeBe}_5$ . . . . .  | 20 |
| 9.  | a) Normal geometry for electron attenuation measurements. b) Electron generation and attenuation geometry for resonant detector with gamma flux incident from the right . . . . .   | 22 |
| 10. | Relationship of effective thickness "seen" by isotopic electron source to actual thickness as "seen" by parallel electron source . . . . .  | 23 |
| 11. | Transmission of electrons from isotropic electron source at a specified depth in an infinitely thick $\text{FeBe}_5$ foil . . . . .   | 24 |
| 12. | a) Signal-to-baseline (background). b) Detector efficiency as a function of iron-57 abundance for a ten foil detector with a total thickness of two resonant half values, assuming $f_s = f_D = .95$ . . . . .  | 26 |

13. a) Signal-to-baseline (background) ratio.  
 b) Detector efficiency as a function of the number of foils for a total thickness of half value layers (3,716 Å) of iron-57 enriched FeBe<sub>5</sub> . . . . . 27
14. a) Signal-to-baseline (background) ratio.  
 b) Detector efficiency as a function of total thickness of foil(s) for 97 percent iron-57 abundance. One resonant half value layer = 1,858 Å, one photoelectric hvl = 239 resonant hvls. n = number of foils . . . . . 29
15. Detector efficiency as a function of total thickness of foil(s) for 50 percent iron-57 abundance. One resonant half value layer (hvl) = 3,604 Å; one photoelectric hvl = 123 resonant hvls. n = number of foils . . . . . 30
16. a) and b) Detector efficiency as a function of total thickness of resonant foils, expressed in resonant half value layers, for 3 percent iron-57 abundance. One resonant half value layer = 60,069 Å; one photoelectric hvl = 7.4 resonant hvls. n = number of foils . . . . . 31
17. a) Line profile for source and absorber using a conventional detector. b) Line profile for a moving absorber between a stationary source and resonant detector . . . . . 34
18. Pulse-height spectrum of tritium loaded gel. Endpoint is at 18.1 keV . . . . . 37
19. Mössbauer spectrum of <sup>119</sup>SnO<sub>2</sub> dispersed in scintillation gel and moving <sup>119m</sup>Pd<sub>3</sub><sup>119m</sup>Sn source. Peak is barely visible at -2.2 mm/s . . . . . 38
20. Pulse-height spectrum of gel scintillation counter. Upper spectra: H.V. = 2000 volts, upper curve with, lower curve without source. Lower spectra: same, but H.V. = 1200 volts . . 38
21. Coincidence arrangement for gel scintillation detector. Photomultiplier tubes are shielded from direct gamma radiation . . . . . 39
22. Mössbauer spectrum of <sup>119</sup>SnO<sub>2</sub> dispersed in scintillation gel and Pd<sub>3</sub><sup>119m</sup>Sn source, using coincidence noise suppression . . . . . 40

|  | <u>PAGE</u> |
|--|-------------|
| 23. Isometric view of proportional counter with top plate removed . . . . .  | 41          |
| 24. Pulse-height spectra for Co-57 Mössbauer source as a function of position on 3 inch x 3 inch window . . . . .  | 42          |
| 25. Photograph of detector for conversion electrons . . . . .  | 44          |
| 26. Diagram of detector for conversion electrons . . . . .   | 44          |
| 27. Pulse-height spectra of a <sup>55</sup> Fe (5.5 keV endpoint) and <sup>57</sup> Co (7.3 keV endpoint) source placed inside the detector . . . . .                    | 45          |
| 28. Mössbauer spectrum of the resonance detector with a 0.5 mil 50 percent enriched stainless steel foil and moving <sup>57</sup> Co in stainless steel source . . . . . | 46          |
| 29. Energy distribution of photoelectrons and conversion electrons obtained by source-detector off resonance (a) and in resonance (b) . . . . .                          | 47          |
| 30. Energy distribution of the conversion electrons from a 0.5 mil 50 percent enriched stainless steel foil . . . . .  | 48          |
| 31. Differential signal/noise of the electrons generated in the stainless steel resonant detector. Optimum selection would be from 2 to 6 keV . . . . .                  | 49          |

LIST OF TABLES

LIST OF TABLES

|   |    |
|---|----|
| 1. Photoelectric cross sections (barns) . . . . . | 16 |
| 2. Compton cross sections (barns) . . . . .       | 16 |

PRELIMINARY STUDY ON THE CHARACTERISTICS AND DESIGN  
PARAMETERS FOR A MÖSSBAUER RESONANT DETECTOR

J. J. Spijkerman, J. C. Travis, P. A. Pella  
and J. R. DeVoe

Progress in the design and fabrication of a resonant detector for Mössbauer Spectroscopy is described. This report begins with a review of all of the methods of detection for this spectroscopy and describes the expected advantages of the resonant detector. If one uses conversion electron detection, considerable enhancement in signal to noise ratio and decrease in linewidth may be realized. Efforts to produce an iron bearing resonant material are described.

Key words: Conversion electrons; iron;  
Mössbauer Spectroscopy;  
resonant detector.

## 1. INTRODUCTION

Conventional type Mössbauer spectrometers use low energy gamma-ray detection systems. Although these counters have a high counting efficiency, their resolution is very poor, typically about 1 keV, compared to the energy width of  $10^{-8}$  eV for the Mössbauer radiation. Since Mössbauer sources are not monochromatic, the resolution of the counter determines the amount of unwanted background radiation. Figure 1 shows a typical spectrum of a  $^{57}\text{Co}$  source near the 14.4 keV Mössbauer radiation which consists of three major components; a) the  $10^{-8}$  eV wide recoil free radiation, b) the  $2 \times 10^{-3}$  eV wide recoil broadened radiation and c) a wide band of Compton and photoelectric effect radiation (degradation products) arising from the 122 keV precursor radiation. Most of the Compton background is generated by the counting gas and walls of the proportional detector or by the scintillating material in a scintillation detector.

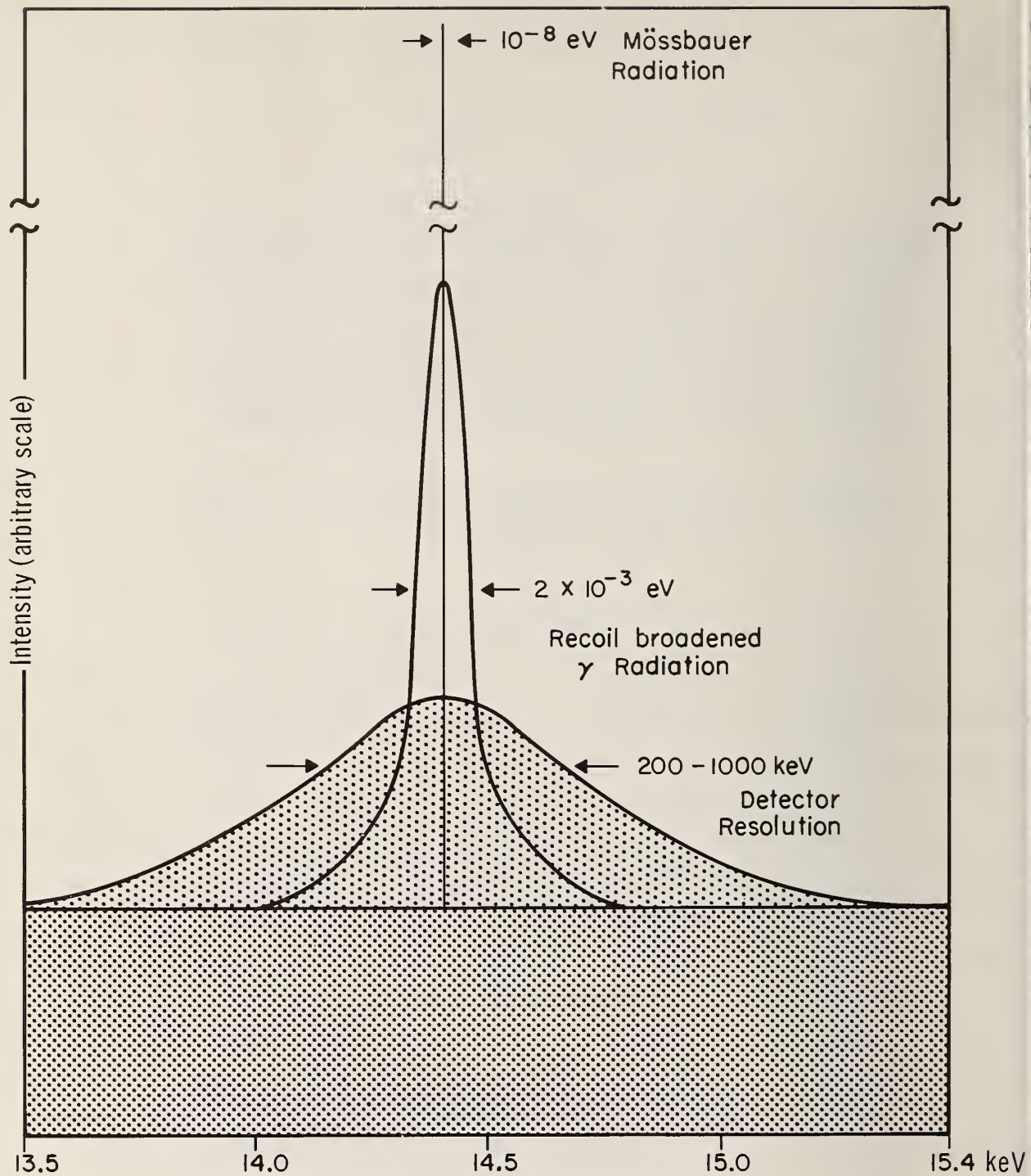


Figure 1. Energy resolution of the various types of processes associated with the 14.4 keV gamma radiation of cobalt-57.

Much of the background radiation in Mössbauer spectroscopy can be suppressed by using a resonant detector. The possibility of using a resonant detector was first discussed at the Allerton Park Mössbauer Conference and several Russian papers on this type of detector have been published [1-9]. The principle of its operation is based upon the detection of internal conversion electrons emitted by resonance-excited nuclei in a detector. Since this detector makes use of the Mössbauer effect, its resolution is near  $10^{-8}$  eV. The background in this type of detector arises from secondary photoelectrons. The process of decay of the 14.4 keV excited nuclear level in iron-57 is shown schematically in Figure 2. For every 100 nuclei in the 14.4 keV excited state ten nuclei decay by emitting the 14.4 keV gamma-ray, and the other 90 nuclei decay by the internal conversion process (e.g. the internal conversion coefficient is 9). This means that a K shell electron is emitted with approximately 7.3 keV energy. An electron from the L shell enters the K shell and emits the characteristic 6.45 keV x-ray. Of these 90 - 6.4 keV x-rays, approximately 63 cause 5.6 keV electrons to be emitted by the Auger effect, and the remaining 27 - 6.4 keV x-rays leave the atom. M to L cascade produces < 1 keV x-rays. Internal conversion with the L shell occurs, but with significantly less probability. Because of the fact that out of 90 - 7.3 keV conversion electrons emitted there are simultaneously 63 - 5.6 keV Auger electrons, the probability for electron detection is enhanced.

The resonant counter can be operated in two modes; a) by placing the material to be analyzed inside the detector, b) by using a stationary source and resonant detector and moving an absorber placed between the source and detector. The first method has the advantage that very small samples ( $10 \mu\text{g}/\text{cm}^2$  of iron) can be used, which in most cases is a surface measurement. Because of the small sample, self-absorption broadening is absent and the spectrum shows very narrow lines predicted by the thin absorber limit. Because of the small sample, the

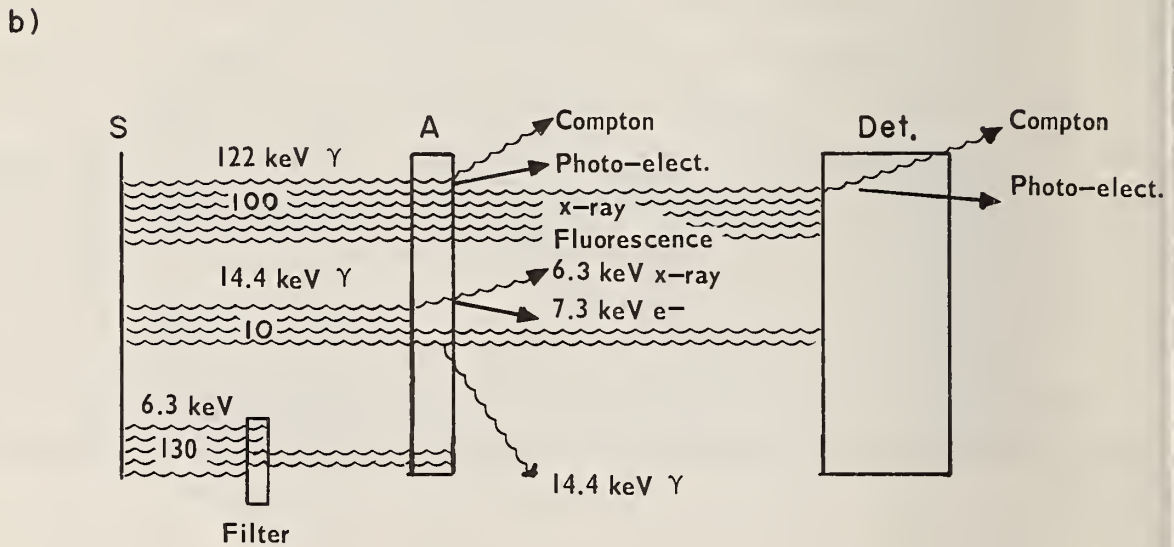
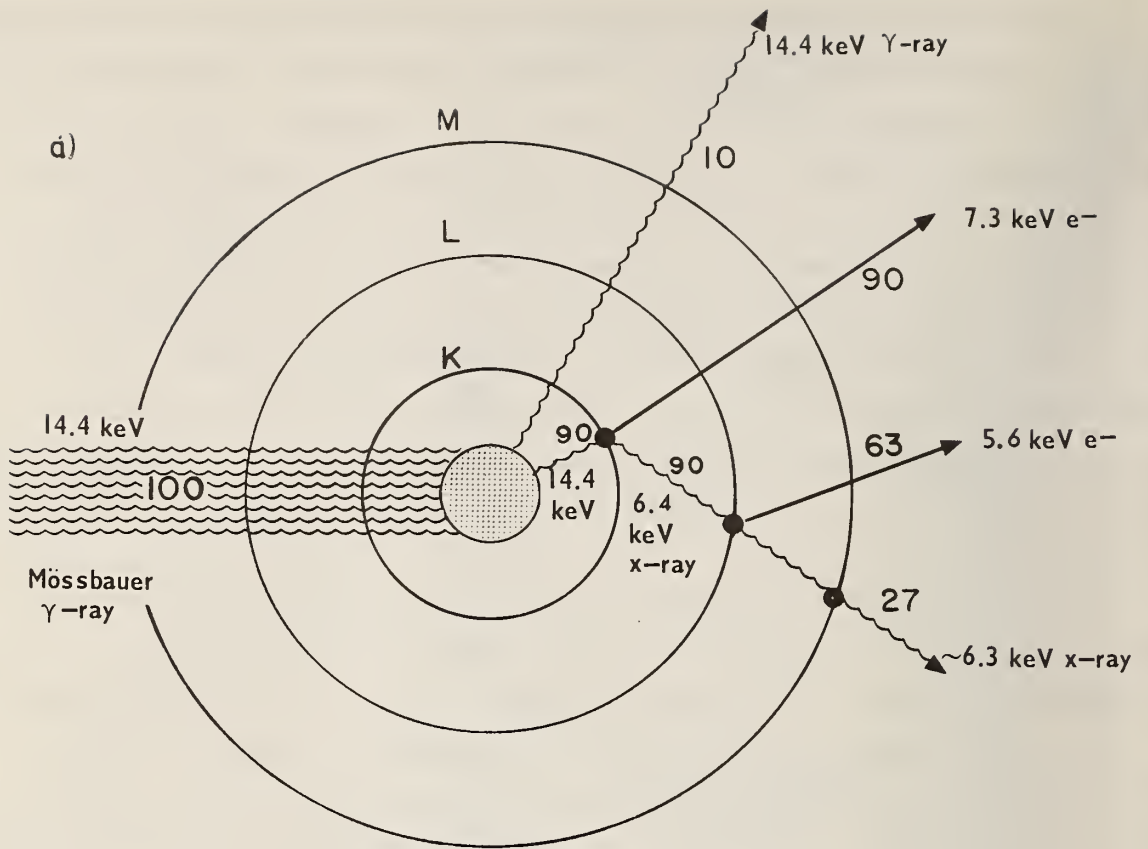


Figure 2. a) Schematic of internal conversion process for the 14.4 keV transition of  $^{57}\text{Co}$ . b) Energy degradation process for a source, absorber and detector system in a conventional Mössbauer detection system.



efficiency is poor, which is partially compensated by the high signal/noise ratio, so that the data accumulation time may approximate that obtained for conventional detectors. The second method has many advantages, but the detector is difficult to fabricate. To obtain maximum efficiency and resolution, the source and absorber must be in resonance at zero relative velocity, with a very narrow resonance profile. Furthermore, the counter material must be of low Z to reduce the Compton background. The efficiency can be increased by using enriched  $^{57}\text{Fe}$  and several converter plates. The resolution of the second method is greatly improved, due to the selective absorption of the counter. For a thin absorber, the line width is reduced by 26 percent. Since the Mössbauer cross section is 200 times the photoelectric cross section, a large reduction in data accumulation time is expected.

## 2. DETECTION METHODS FOR MÖSSBAUER SPECTROSCOPY

For comparison, the different methods used for detection of the Mössbauer effect will be described.

### A. Conventional Transmission Method

The conventional technique, shown in Figure 3a uses a proportional, scintillation or solid state detector. The proportional and scintillation counters have a very high counting efficiency, and can be used at high counting rates, but have poor energy resolution. The solid state detector has better energy resolution, but the counting rate is much lower, hence the data accumulation time is longer. The Compton and photoelectric effect background accounts for the large background,  $B_p$ . If a very thin sample is used, most of the radiation will pass through the sample; and the baseline B will increase, and the effect will decrease. For a thick sample, the atomic absorption by the sample will attenuate the Mössbauer radiation, but not the higher energy radiation present, and the Compton and photoelectric effect background will increase. Shimony [10] and Protop and Nistor [11] have derived the optimum conditions for the sample thickness with background radiation.

### B. Conventional Scattering

The resonantly scattered 14.4 keV gamma ray can be detected by the conventional low energy gamma-ray detector. Because of internal conversion, the efficiency for detecting the Mössbauer effect is low, and the background is significant due to the Compton and photoelectric effect in the absorber produced by the 122 keV precursor gamma ray.

The geometrical arrangement is very important for overall efficiency. A recently developed toroidal counter greatly increases the geometrical efficiency [12]. Shielding of the source is also essential to reduce the background, and depleted uranium gives the best total attenuation for shielding. Pene-

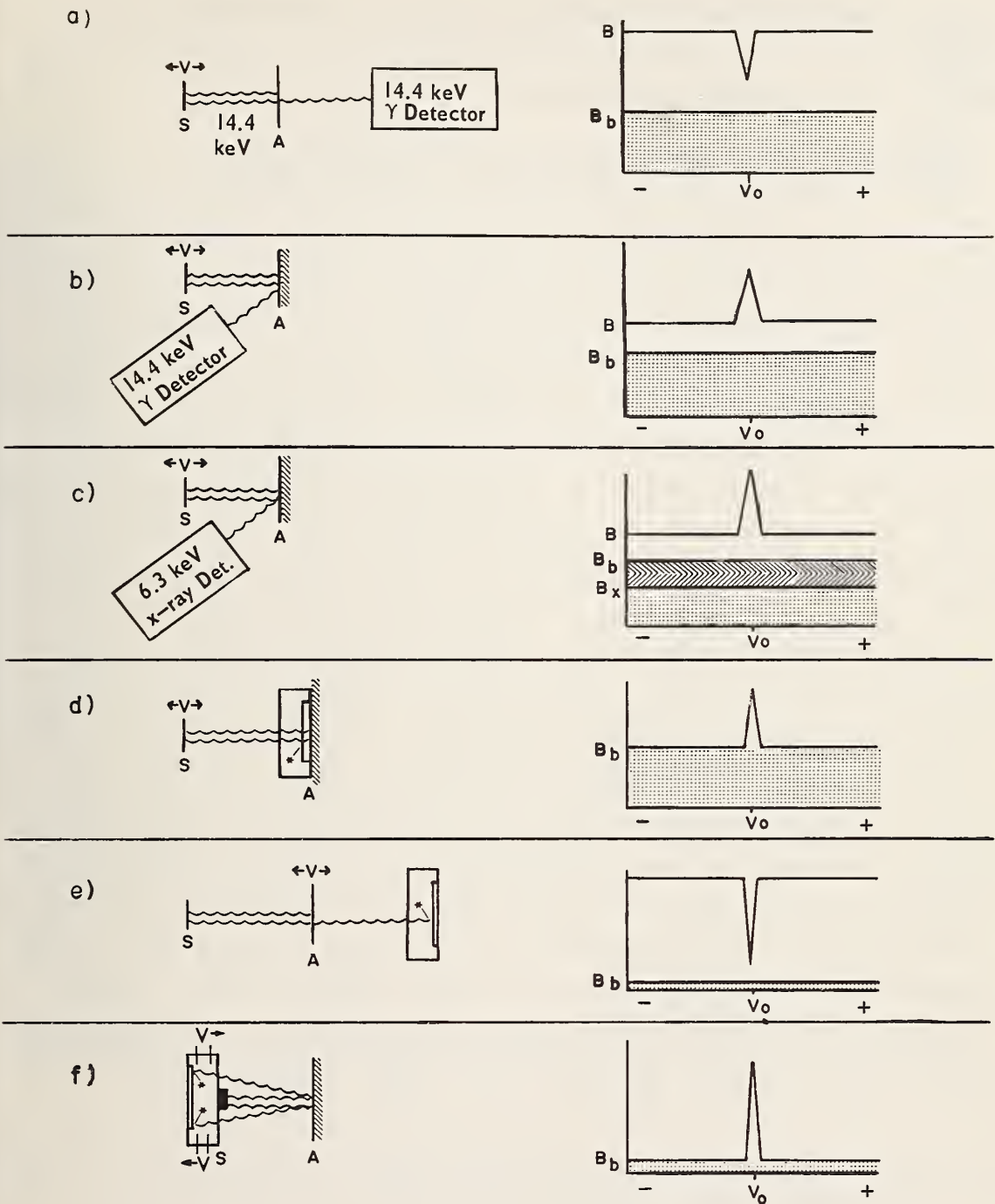


Figure 3. Detection methods for Mössbauer spectroscopy. a) Conventional transmission. b) Conventional scattering. c) Conversion x-ray scattering. d) Conversion electron scattering. e) Transmission, using a resonant detector. f) Scattering, using a resonant detector.

tration depth into the sample is about .5 mils\* [13]. The observed line width is broadened due to self-absorption in the sample of the reemitted Mössbauer radiation.

### C. Scattering with Detection of Conversion X-Rays

The low detection efficiency of the conventional scattering method can be improved by detection of the conversion x-rays. Since the K conversion is 90 percent with about a 30 percent fluorescent yield, a 270 percent increase in efficiency is observed. For iron, the attenuation of the 6.3 keV x-ray radiation by the sample is the same as that of the 14.4 keV, due to the K absorption edge at 7.1 keV. Mass absorption coefficients as a function of element are given in Figure 4. The use of x-ray detection also eliminates the possibility of detecting reabsorbed resonantly scattered Mössbauer radiation by the sample, and a narrower linewidth is observed. The penetration depth in the sample has been calculated by [14], and the amplitude of the backscattered radiation as a function of thickness is shown in Figure 5.

To determine the sample depth that enters into an iron-57 Mössbauer scattering spectrum when 6.3 keV x-rays are being counted, two spectra were obtained for a sample consisting of a stainless steel foil 0.001 inch thick covered with iron foil. For one spectrum the thickness of iron foil was 0.5 mil. The Mössbauer scattering spectra are shown in Figure 6. Argon with 10 percent methane was used for a flow gas, to reduce the Compton effect in the detector. As seen in Figure 6, the central peak, which is due to the underlying stainless steel foil, decreases in relative intensity as the thickness of iron covering the stainless steel is increased. The calculated areas beneath the iron and stainless steel peaks show that 78 percent of the backscattered signal is from the first 0.2 mil

---

\* SI system of units requires conversion to meters (multiply by  $2.54 \times 10^{-5}$ ). This conversion should be made at other similar entries in this report.

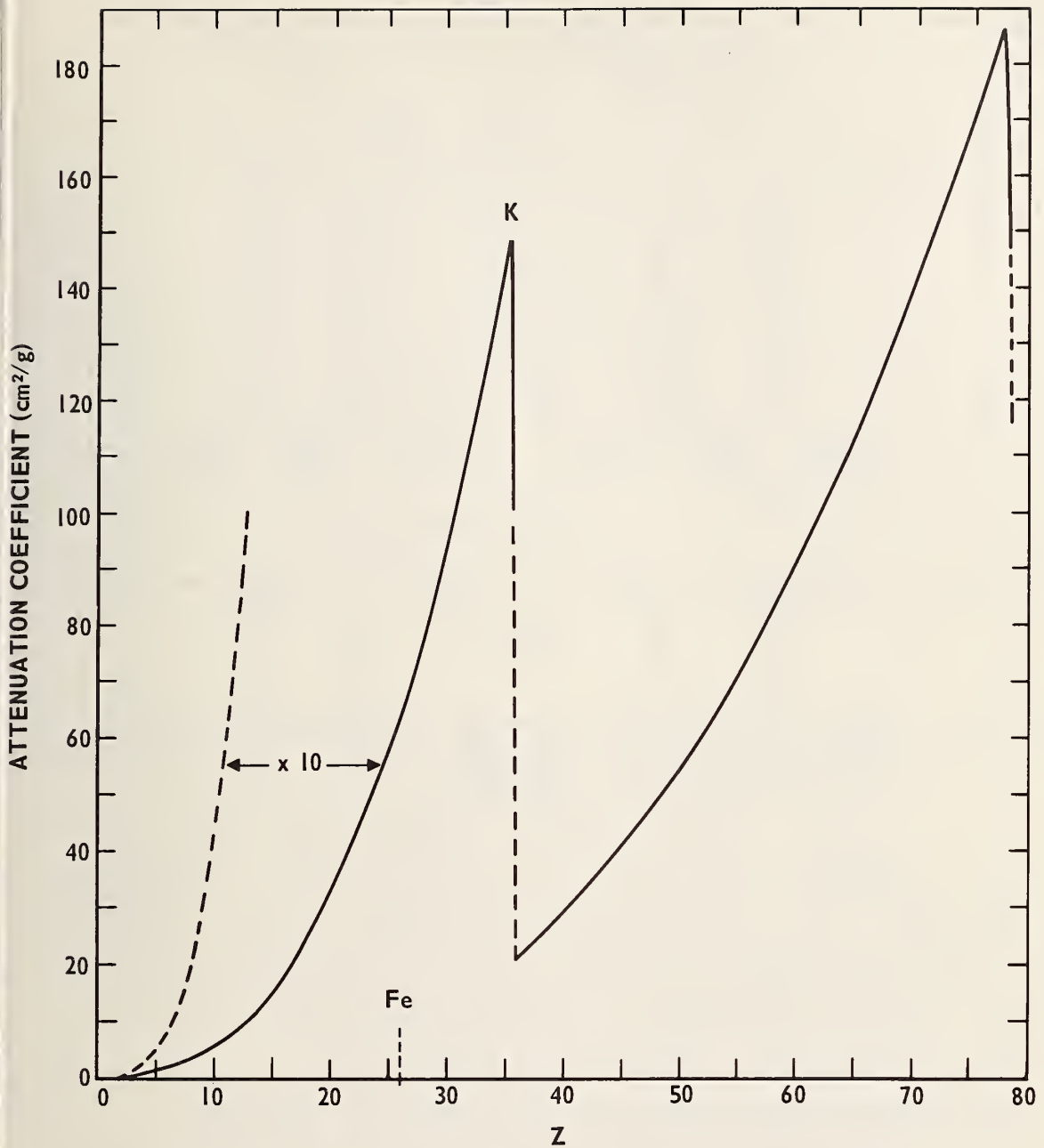


Figure 4. Attenuation coefficient for 14.4 keV gamma radiation as a function of element [19].

of the sample depth and that 93 percent of the backscattered signal originates in the first 0.5 mil of sample depth. These figures are in general agreement with those predicted by Terrell and Spijkerman [14]. For all practical purposes, an iron-57 Mössbauer backscattering spectrum obtained by detecting the

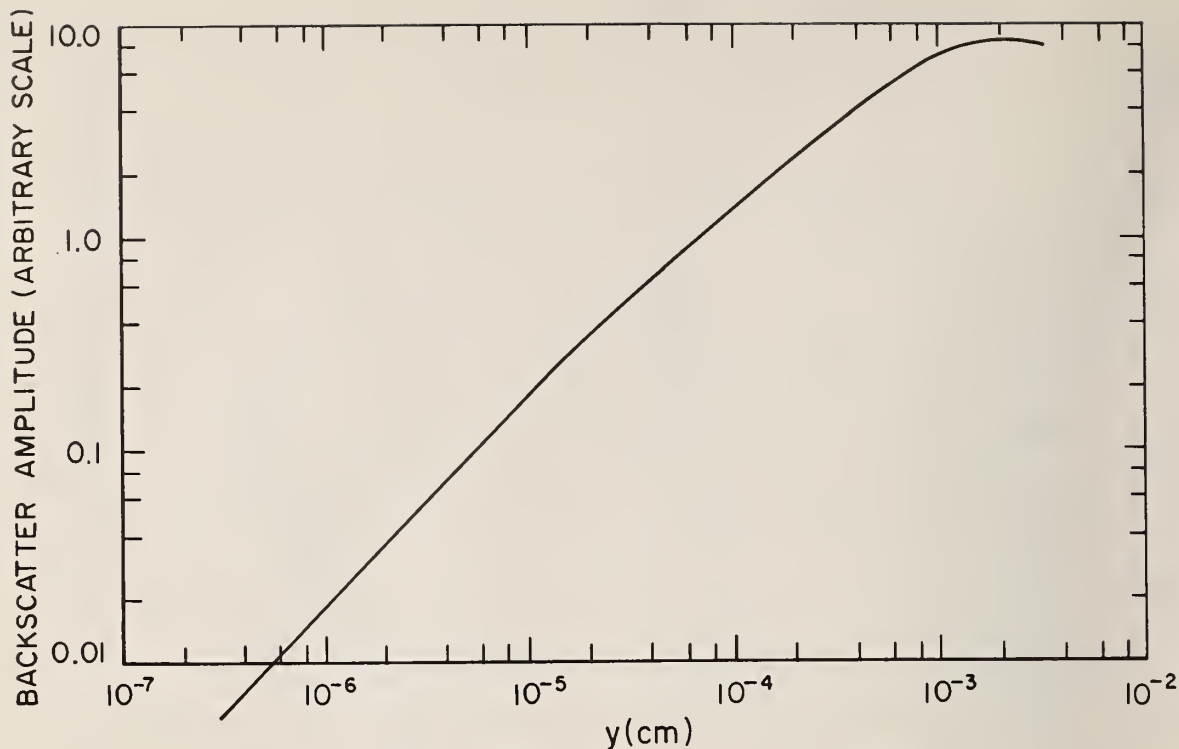


Figure 5. Number of 6.3 keV internal conversion x-rays from Fe as a function of the penetration into the sample for backscattering geometry.

6.3 keV x-rays resulting from internal conversion of the 14.4 keV Mössbauer gamma rays represents a layer of sample approximately 0.5 mil thick. A major background contribution is the 6.3 keV x-ray fluorescence in the absorber resulting from the 122 keV precursor, as shown in Figure 3c.

#### D. Scattering with Detection of Conversion Electrons

The third method for the detection of the scattered Mössbauer radiation is by conversion electron detection [15]. It can be seen from Figure 2 that this conversion process is 90 percent efficient, resulting in 7.3 keV electrons followed 70 percent of the time by 5.6 keV Auger electrons.

The range of these conversion electrons in solids is very short which limits the sample depth that is effective in producing a Mössbauer spectrum. To determine the sample depth, two

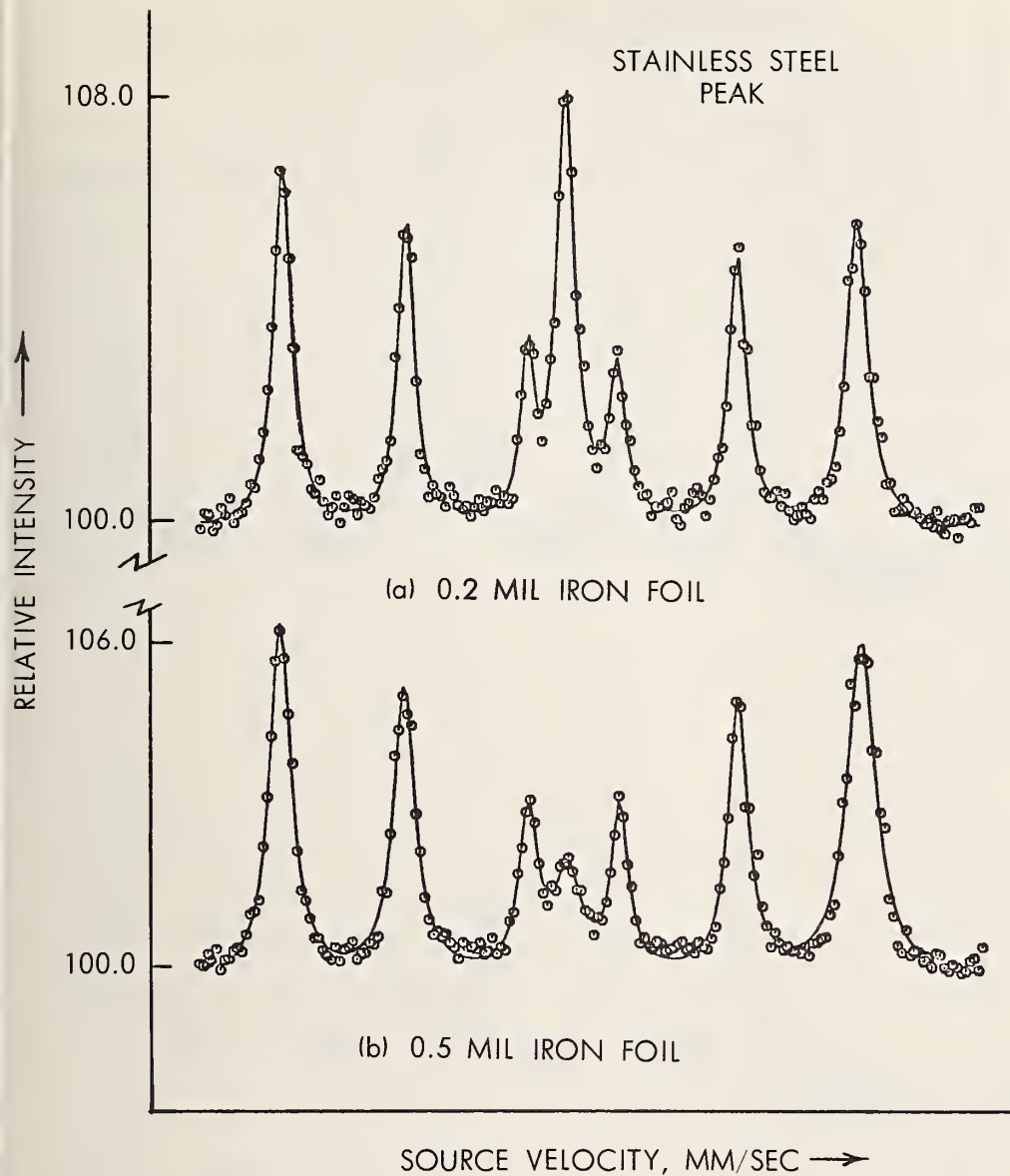


Figure 6. X-ray detection Mössbauer scattering spectra for iron foil on stainless steel foil.

one-mil-thick stainless steel foils were covered with  $600 \text{ \AA}$  and  $3000 \text{ \AA}$  respectively of vacuum deposited iron and placed inside the detector. Helium-10 percent  $\text{CH}_4$  flow gas was used to detect the conversion electrons and discriminate against x-ray and gamma-ray detection. The two spectra are shown in Figure 7. The calculated areas for the iron peaks and stainless steel peak show that 65 percent of the intensity originates within the first  $600 \text{ \AA}$  and 96 percent within the first  $3000 \text{ \AA}$ . The

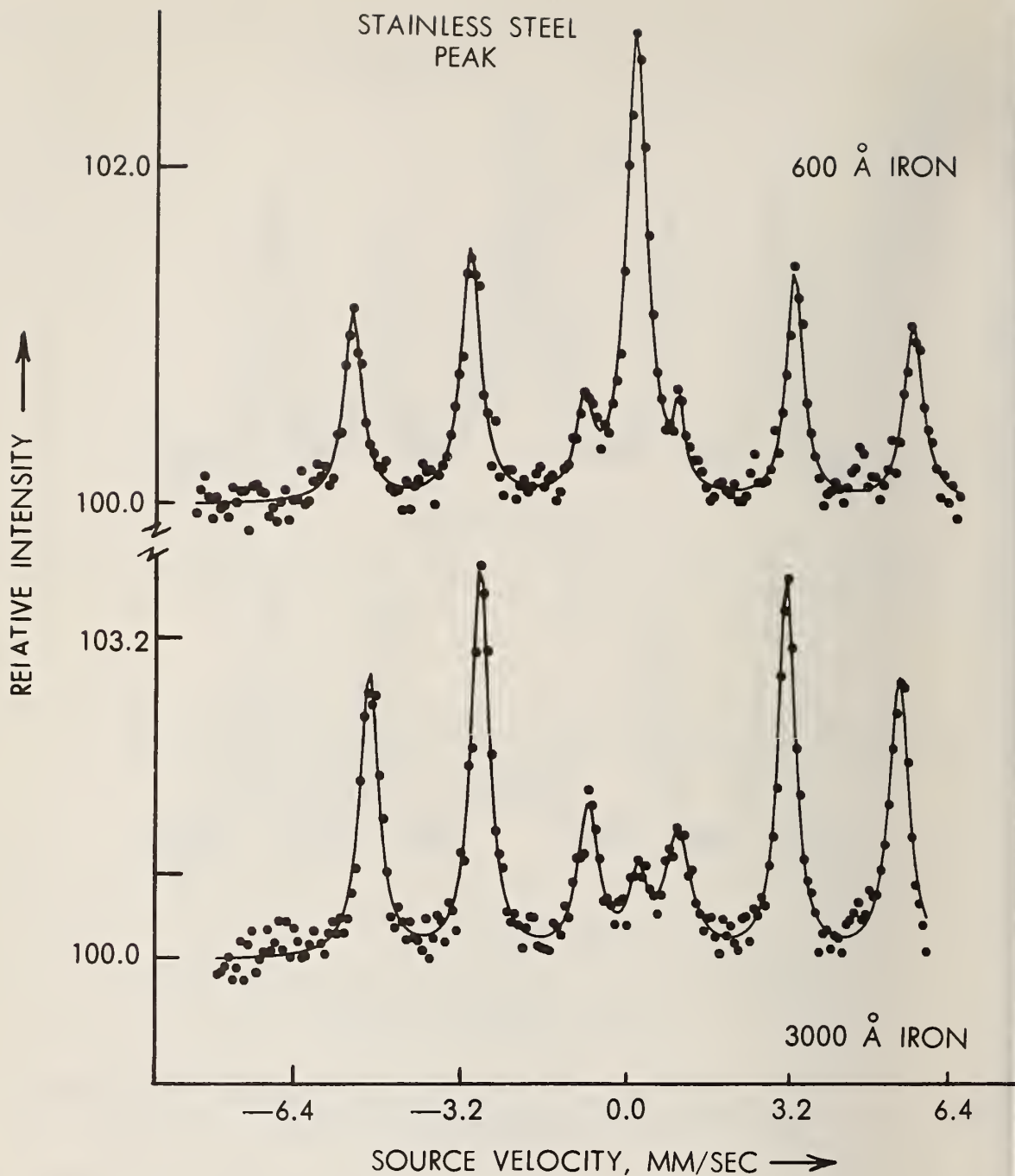


Figure 7. Conversion-electron detection Mössbauer back-scattering spectra for vacuum-deposited iron on stainless steel foil.

geometrical efficiency for this detection method is nearly 50 percent which makes this method ideal for surface analysis of iron bearing materials.



#### E. Transmission Using a Resonant Detector

The conversion electron detector described in D can be used for Mössbauer transmission measurements [16], as shown in Figure 3e. While in transmission geometry using a conventional detector, the movement of the source or absorber is entirely equivalent, this is not the case for a resonant detector. The source and the conversion plate (absorber) must be in resonance at zero relative velocity, and a moving absorber placed between the stationary source and the detector is used. To increase the detection efficiency of the counter, several iron-57 enriched converter plates should be used. The extremely high energy resolution of the detector greatly reduces the background, and the selective absorption by the detector reduces the observed linewidth by 27 percent compared to a nonselective (conventional) detector [8]. The background is caused by the photoelectric effect, and therefore, the detector's geometrical design and selection of materials must be carefully considered to minimize this effect. Since the background is greatly reduced, the detector can be used with much stronger sources before counting rate saturation occurs. Such saturation is a serious limitation with the conventional detector.

#### F. Scattering Using a Resonant Detector

The same arguments considered in the previous section (E) hold for this case. Since it is desirable to analyze bulk material nondestructively, the source and detector have to be moved in opposite directions in order to obtain zero relative velocity. The small physical dimensions of this detector present no difficulty with the available Mössbauer spectrometers. Sample penetration depth is the same as discussed in Section B (0.5 mils). With the low background of this detector, the improved Mössbauer spectral resolution, and the possibility of using much stronger sources, the data accumulation times can be greatly reduced.

### 3. THEORY

#### A. Internal Conversion Electrons

The ideal detector for Mössbauer spectroscopy would be one which generates a pulse for every incoming recoil-free photon from the source, but does not respond to any other incoming radiation. In principal, the best discrimination between recoil-free photons and other radiation is provided by an absorber in resonance with the source such that incoming recoil-free photons are signalled by resonance absorption events. The principal problem encountered in incorporating this principal into a detector, however, is the requirement that resonant absorption events in the detector, and only such events, be translated into an electronic signal suitable for counting.

In iron-57, every one hundred resonant absorption events are followed in  $10^{-7}$  seconds by a distribution of reemitted radiation consisting roughly of ten 14.4 keV gamma photons, ninety 7.3 keV internal conversion electrons, twenty seven 6.3 keV x-rays, sixty three 5.5 keV Auger electrons, and a cascade of low energy x-rays and Auger electrons. Electron counting to signal the occurrence of resonant absorption events obviously yields the highest efficiency, or fraction of incoming signal detected, by virtue of the numbers available. In addition, a gas filled counter may be built with a high cross section for electrons, but very low cross section for incoming gamma and x-radiation, minimizing the background from external sources. Discounting electronic noise, the primary source of unwanted counts would be photoelectrons and Compton electrons created inside the detector by incoming radiation. With appropriate detector optimization, such background may be kept to a small fraction of the signal.

#### B. Cross Sections

Theoretical estimates of detector discrimination and efficiency, for optimization purposes, require consideration of the processes which produce electrons and the probability of the

electrons escaping from the foil to be detected by the gas. For radiation of the energy range of interest to us, the only significant contributions to electron production are Compton, photoelectric, and resonant interactions. For the Compton and photoelectric effects, the number of electrons produced per  $\text{cm}^2$  in a layer of thickness  $\Delta t$  at depth  $t$ , say  $\Delta N_c$  and  $\Delta N_p$ , may be expressed as

$$\Delta N_{Ci} = \mu_{Ci} I_i(t) \Delta t$$

$$\Delta N_{pi} = \mu_{pi} I_i(t) \Delta t$$

(1)

$$\Delta N_c^{\text{tot}} = \sum_i \Delta N_{Ci}, \quad \Delta N_p^{\text{tot}} = \sum_i \Delta N_{pi}$$

$$\{E_i\} = \{14.4, 122, 136\}$$

where  $I_i(t)$  is the number of photons per  $\text{cm}^2$  of energy  $E_i$  incident on the layer of depth  $t$ , and  $\mu_{Ci}$  and  $\mu_{pi}$  are the energy dependent Compton and photoelectric linear attenuation coefficients. For an intermetallic foil, the linear attenuation coefficients may be obtained from the cross sections characteristic of the various metals included,

$$\mu = \sum_i n_i \sigma_i \quad (2)$$

where  $n_i$  is the number of atoms/ $\text{cm}^2$  and  $\sigma_i$  is the interaction cross section, in  $\text{cm}^{-2}/\text{atom}$ , of the  $i$ th species.

Approximate expressions for the photoelectric and Compton cross sections as functions of  $E_\gamma$ ,  $Z$  (absorber foil atomic number) and  $E_k$ , the K shell absorption edge, as given by Berthelot [17], have been used to calculate representative cross sections for iron and beryllium, as shown in Tables 1 and 2 in units of 1 barn =  $10^{-24} \text{cm}^2$ .

Table 1. Photoelectric cross sections (barns).

| Z \ hv | 14.4    | 122     | 136   |
|--------|---------|---------|-------|
| 4      | 2.69    | .0018   | .0012 |
| 26     | 8450.00 | 12.2000 | 8.5   |

Table 2. Compton cross sections (barns).

| Z \ hv | 14.4  | 122   | 136   |
|--------|-------|-------|-------|
| 4      | 2.52  | 2.18  | 2.22  |
| 26     | 16.39 | 14.16 | 14.46 |

The number of internal conversion electrons produced per  $\text{cm}^2$  by Mössbauer interactions in a layer of thickness  $\Delta t$  at depth  $t$ ,  $\Delta N_{IC}$ , is given by

$$\Delta N_{IC} = \mu_r I_r(t) \Delta t \frac{\alpha}{1+\alpha} \quad (3)$$

$$\alpha = 9$$

where  $\alpha$  is the internal conversion coefficient, and where  $I_r(t)$  is the number of recoilless photons per  $\text{cm}^2$  reaching depth  $t$ . The resonant linear attenuation coefficient,  $\mu_r$ , is given by

$$\mu_r = n_{Fe} a_D f_D \frac{\sigma_o}{1 + \left(\frac{S}{\Gamma}\right)^2}$$

$$\sigma_o = 2.2 \times 10^{-18} \text{ cm}^2 \quad (4)$$

$$\Gamma = \Gamma_S + \Gamma_D \simeq .15 \text{ mm/sec}$$

where  $n_{\text{Fe}}$  is the number of iron atoms per  $\text{cm}^3$ ,  $a_{\text{D}}$  is the iron-57 isotopic abundance and  $f_{\text{D}}$  is the recoilless fraction of the detection foil(s),  $S$  is the isomer shift between the centers of the source and detector lines, and  $\Gamma_{\text{S}}$  and  $\Gamma_{\text{D}}$  are the source and detector halfwidths.

In addition to the "primary" electrons created by the three absorption processes, the K fluorescence yield of about .3 for iron means that about 7 Auger electrons are emitted for every ten ejected K electrons. Thus, for a pure iron detector foil, the total number of electrons created is given by

$$1.7 \left( \sum_i \Delta N_{\text{Ci}} + \sum_i \Delta N_{\text{pi}} + \Delta N_{\text{IC}} \right)$$

For an intermetallic foil, the numbers of electrons created in each species would need to be tallied separately to keep proper account of the different Auger electron yields of the different metals.

Equations (1) and (3) account for the number of primary electrons produced at depth  $t$  as long as the total photon flux at that depth,  $I_i$ , and the resonant portion of that flux,  $I_r(t)$ , are known. Therefore, we must account for photons removed from the beam over each increment,  $\Delta t$ , as well as electrons created. Neglecting secondary Compton photons, we may say that one photon is removed for each primary Compton or photoelectron produced, and ten resonant photons are removed for each nine internal conversion electrons created, or

$$\Delta I_i(t) = - \left( \Delta N_{\text{Ci}} + \Delta N_{\text{pi}} + \frac{1+\alpha}{\alpha} \Delta N_{\text{IC}} \delta_{i0} \right) \quad (5)$$

$$\delta_{i0} = 0 \text{ if } i \neq 0; \quad \delta_{i0} = 1 \text{ if } i = 0$$

where the negative sign denotes a decrease over the interval,  $\Delta t$ . The reduction of the resonant photon beam is somewhat more difficult to describe:

$$\Delta I_r(t) = -\frac{1+\alpha}{\alpha} \Delta N_{IC} + \frac{I_r(t)}{I_o(t)} (\Delta N_{Co} + \Delta N_{po}) \quad (6)$$

The second term on the right implies that the fraction of non-resonantly removed photons which is taken from the resonant photon supply is equal to the fraction of resonant photons in the incident beam. It may be seen from (5) and (6) that, although at depth zero  $I_r(0)/I_o(0) = f_s$ , the source recoilless fraction, the fraction of resonant photons in the  $E_o$  beam,  $I_r(t)/I_o(t)$ , changes with increasing  $t$ . This is a significant point in optimization of efficiency and selectivity.

For  $i \neq 0$  in (5), i.e. for gamma-ray energies other than the Mössbauer line, such as the 122 and 136 keV lines for cobalt-57, (5) may be written

$$\Delta I_i = -(\Delta N_{Ci} + \Delta N_{pi}) = -I_i(t) (\mu_{Ci} + \mu_{pi}) \Delta t \quad (7)$$

$$dI_i = -I_i(t) (\mu_{Ci} + \mu_{pi}) dt$$

which may be integrated to yield the familiar exponential expression,

$$I_i(t) = I_i(0) e^{-(\mu_{Ci} + \mu_{pi})t} \quad (8)$$

For the Mössbauer line, however, the peculiar interplay of equations (5) and (6) would make any analytical expressions for  $I_o(t)$  and  $I_r(t)$  exceedingly cumbersome. Thus, for computational purposes, these values are kept track of numerically by applying the appropriate decrements from (5) and (6) at each layer.

### C. Efficiency

The detector efficiency, the fraction of incoming resonant photons detected, is limited by at least two essentially invariant factors, and numerous variable factors. For iron-57, the internal conversion coefficient of 9 places a limit of 90 per-

cent on the maximum efficiency of a resonant detector relying on conversion electron counting. A second "invariant" factor is the need for a substrate to support the thin foils required. Thus, at least half of the electrons created in even the thinnest of foils would be "lost" into the substrate, for a 50 percent geometrical efficiency limit. The combined limit due to these invariants is thus about 45 percent. The primary efficiency limiting factor which is subject to optimization is the attenuation of the internal conversion and accompanying Auger electrons in exciting the foil. Obviously, only an infinite number of infinitesimally thin films in the counter could reach the 45 percent limit.

In order to set practical limits on the design of the resonant films, it is advantageous to simulate via computer the efficiency behavior of a given resonant material as a function of number and thickness of films, Fe-57 abundance, source-detector shift, and so forth. The calculations on the following pages relate to the alloy  $\text{FeBe}_5$ , with a density of  $3.272 \text{ g/cm}^3$  and a molecular weight of 101. The calculations may be greatly simplified by noting from Tables 1 and 2 that the iron photoelectric cross section for 14.4 keV radiation is orders of magnitude larger than any other cross section. We thus include only this one nonresonant interaction in the computations as a first approximation.

The two interactions being considered, the resonant one and the 14.4 keV iron photoelectric one, give rise to four species of electrons. The primary internal conversion electron has an initial energy given by the difference between 14.4 keV and the 7.1 keV K edge for a value of 7.3 keV. The accompanying x-ray energy is given by the K edge less the .8 keV L edge for a total of 6.3 keV, such that the Auger electron energy is 6.3 keV less the L edge for a total of 5.5 keV.

The iron K shell photoelectrons from the 14.4 keV radiation also carry 7.3 keV of energy, and the accompanying Auger electrons carry 5.5 keV.

Attenuation curves for 5, 10, 15, and 20 keV electrons in copper and gold have been given by Cosslett and Thomas [18]. Expressed in thickness units of  $\text{g}/\text{cm}^2$ , the copper and gold results are surprisingly similar. Furthermore, these workers state that the results for aluminum are practically identical with those for copper so that the attenuation curves are essentially  $Z$  independent. For this reason, we have employed the copper results to give the approximate attenuation curves for  $\text{FeBe}_5$ , shown in Figure 8. The curves as shown have been "specialized" to  $\text{FeBe}_5$  by expressing the thickness in angstroms, using the  $\text{FeBe}_5$  density, but it may be generalized to any alloy by applying the density ratio to the thickness scale.

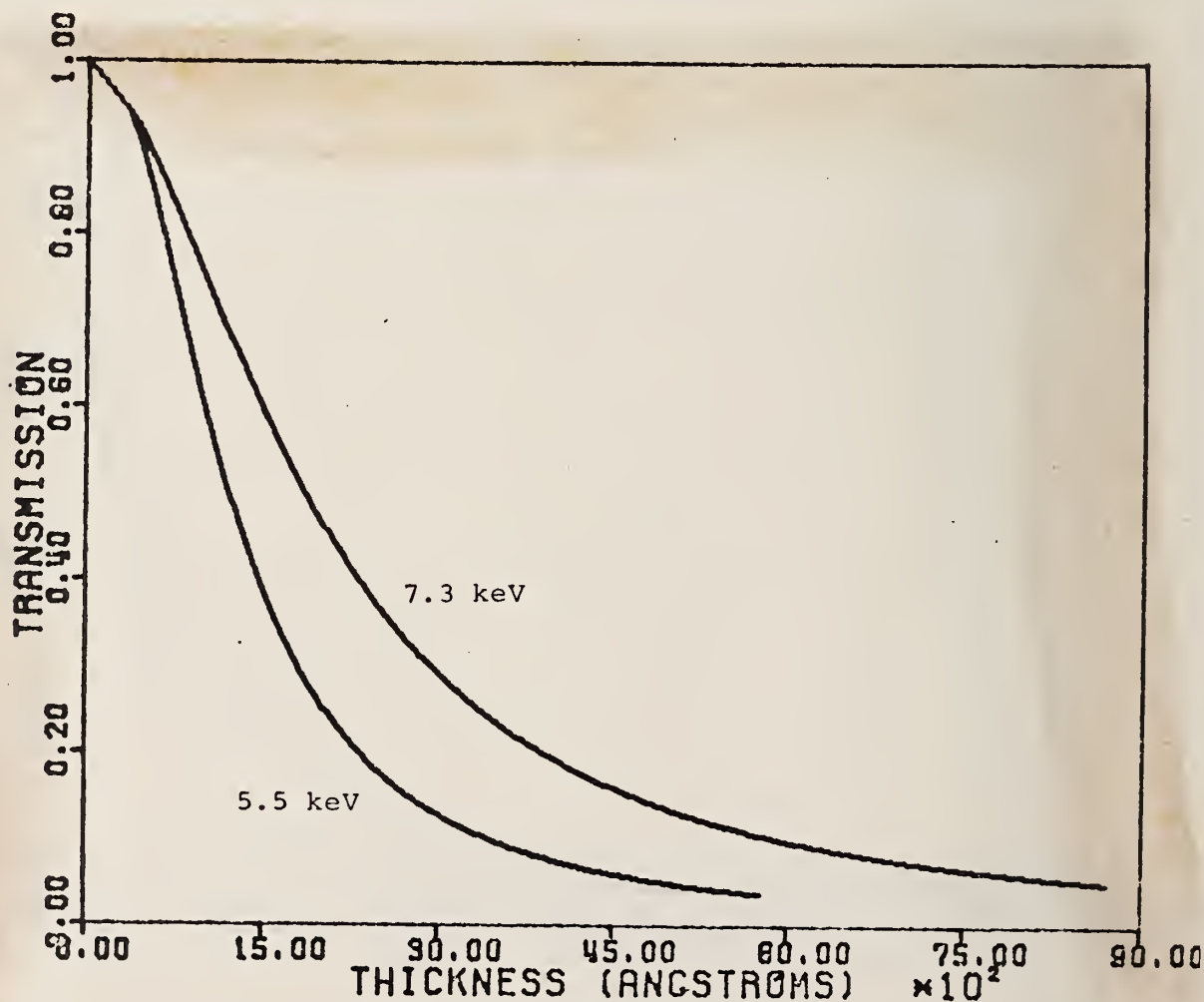


Figure 8. Transmission of parallel electrons through  $\text{FeBe}_5$ .



The curves of Figure 8 were generated by fitting Lorentzian curves to several data points obtained from the 5, 10, and 15 keV data of Cosslett and Thomas [18] by parabolic interpolation. The original data were obtained by impinging parallel beams of electrons of the various energies on a series of foils and recording the total fraction of electrons emerging from the far side of the foil regardless of direction. The distinction between this geometry and that of our experimental arrangement is illustrated in Figure 9, with their geometry shown in 9(a). For our geometry, (9b), we assume as a first approximation that the electrons created at a depth,  $t$ , in a foil have no angular preference (Photoelectrons have a certain bias in favor of the incident photon direction, but this is not very significant for lower energies). Measuring the depth,  $t$ , from the "active" face of the foil (side next to the counting gas as opposed to the substrate) implies that those electrons emitted in a small increment of solid angle at  $\theta = 0$  (where  $\theta$  is measured with respect to the normal to the face of the foil) must travel a distance,  $t$ , to exit the foil, whereas those emitted at an angle  $\theta \neq 0$  must travel a distance  $t \cos \theta$ . (Again, this is an approximation since electrons do not travel straight paths through matter). Considering the electrons to have a maximum range  $R$ , those electrons traveling in a direction for which  $\theta > \cos^{-1}(t/R)$  will not leave the foil. In other words,  $2\pi(1 - t/R)$  steradians of solid angle will contain electrons with a possibility of escaping, compared to the  $4\pi$  steradian emission geometry, so the fraction  $(1 - t/R)/2$  of the electrons have a finite probability of escaping.

To determine a realistic attenuation factor for the fraction of electrons which may escape, we assign an effective depth,  $t_{\text{eff}}$ , in terms of the true depth,  $t$ , and electron range,  $R$ , by finding the expectation value of  $t \cos \theta$  over the solid angle discussed above:

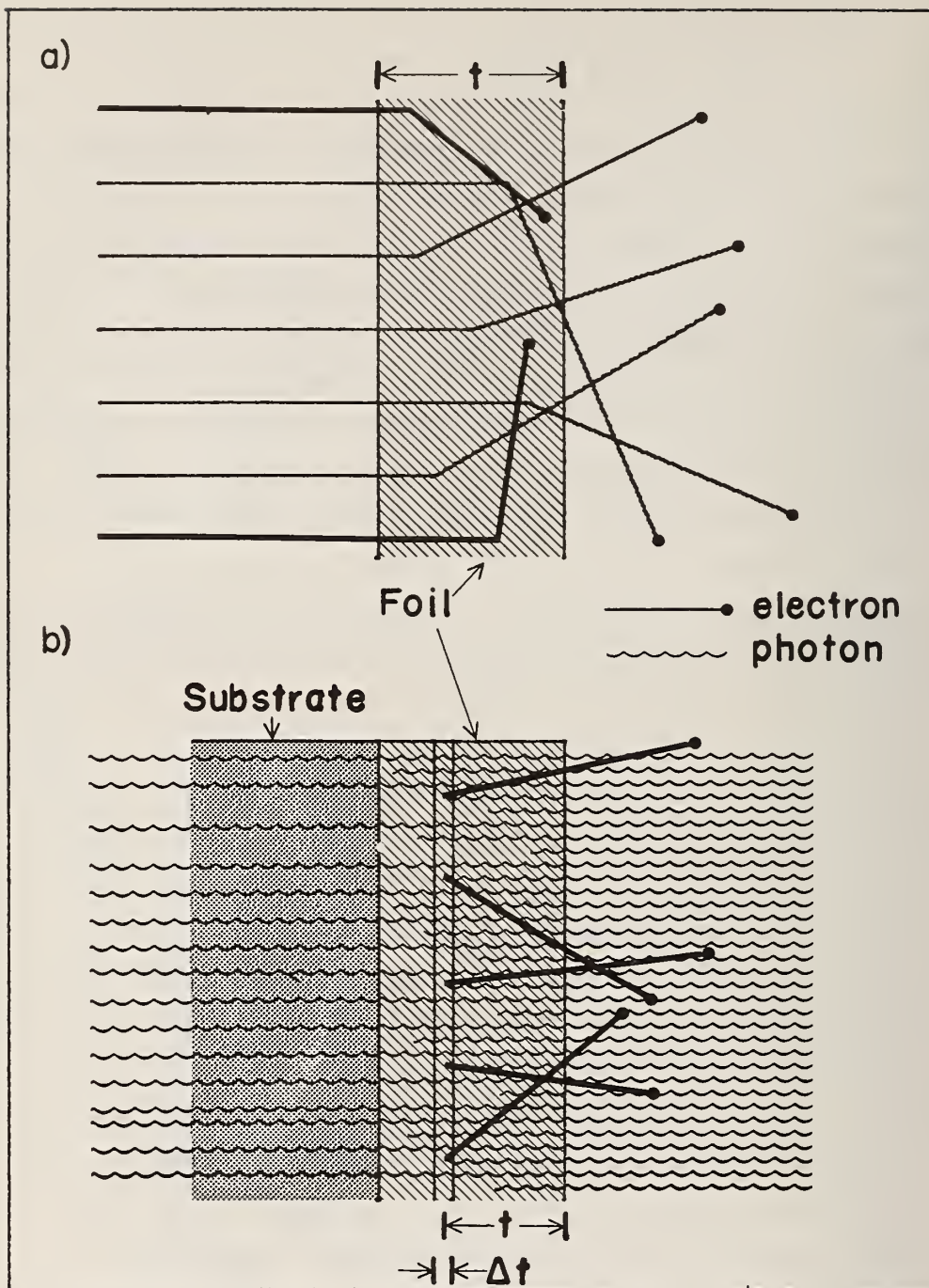


Figure 9. a) Normal geometry for electron attenuation measurements. b) Electron generation and attenuation geometry for resonant detector with gamma flux incident from the right.

$$t_{\text{eff}} = \frac{\int_0^{\cos^{-1}(t/R)} t \cos\theta \sin\theta \, d\theta}{\int_0^{\cos^{-1}(t/R)} \sin\theta \, d\theta} = \frac{t \ln(R/t)}{(1 - t/R)} \quad (9)$$

where  $\sin \theta$ , the weighting factor, is proportional to the number of electrons emitted at angle  $\theta$ , for isotopic emission. Figure 10 shows the relationship of  $t_{\text{eff}}$  to  $t$ , in units of the

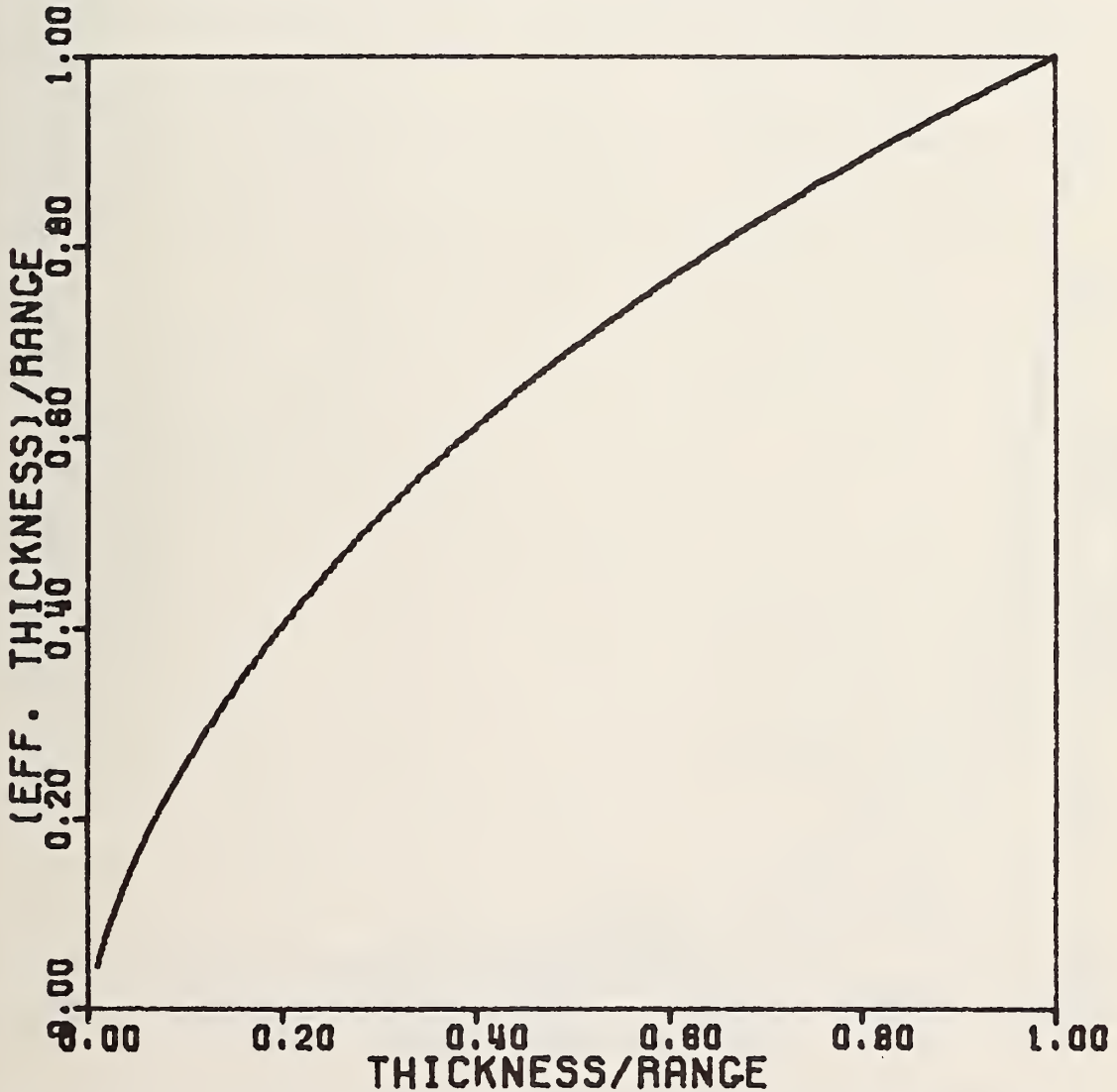


Figure 10. Relationship of effective thickness "seen" by isotopic electron source to actual thickness as "seen" by parallel electron source.

electron range. As might be expected, the two may be seen to be equal for the end points,  $t = 0$  and  $t = R$ . If  $L_1(t)$  and  $L_2(t)$  are the Lorentzian descriptions of parallel electron attenuation, as shown in Figure 8 for the geometry of Figure 9(a), then electron attenuation curves for the geometry of 9(b) may be expressed approximately by

$$L'_1(t) = .5(1 - \frac{t}{R}) L_1(t_{\text{eff}}) = .5(1 - \frac{t}{R}) L_1(t \ln(\frac{R}{t}) / (1 - \frac{t}{R})) \quad (10)$$

The curves  $L'_1$  and  $L'_2$  are shown in Figure 11 for  $\text{FeBe}_5$ .

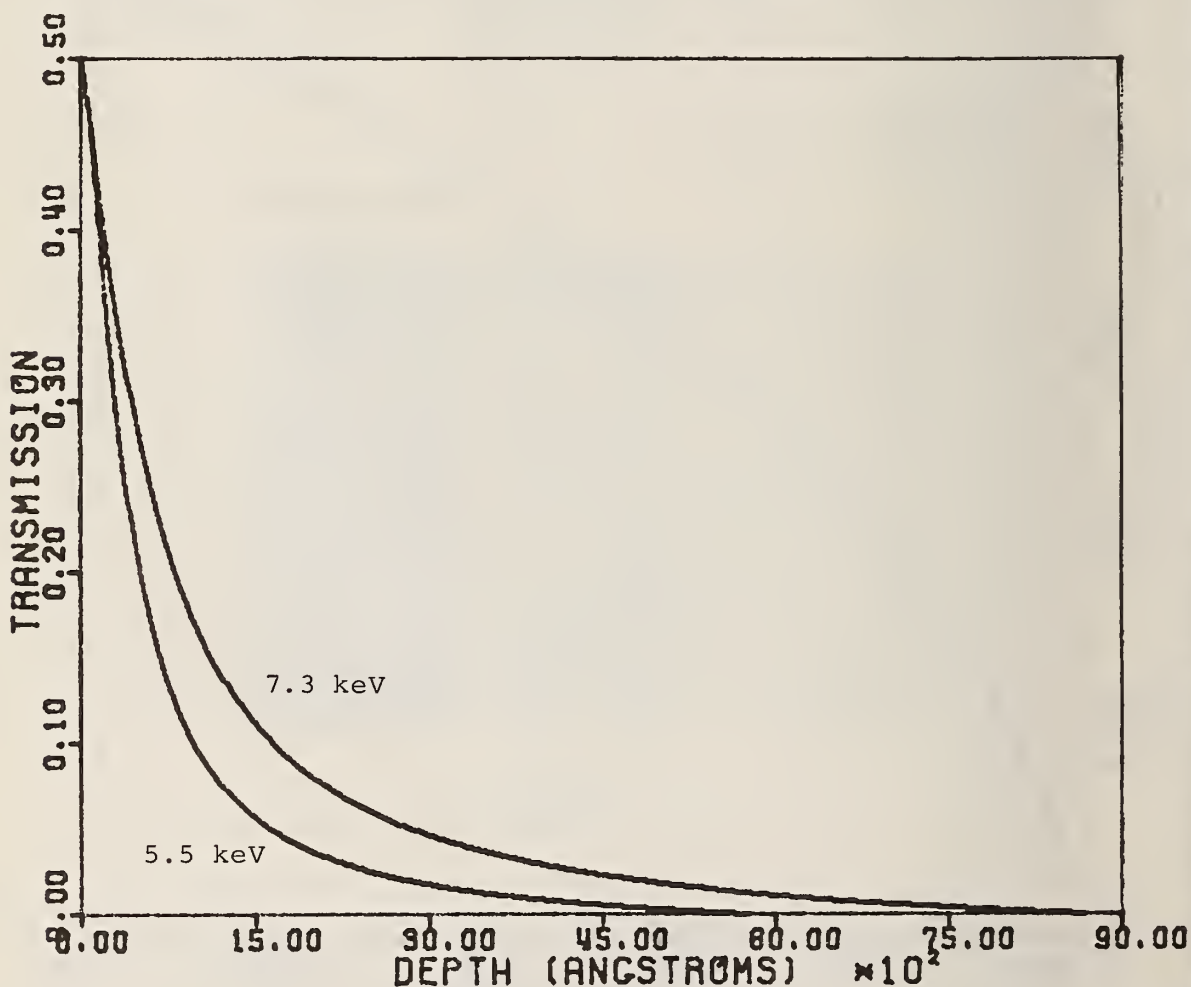


Figure 11. Transmission of electrons from isotropic electron source at a specified depth in an infinitely thick  $\text{FeBe}_5$  foil.

The various equations presented above for photon attenuation, electron production, and electron attenuation, have been incorporated into the computer program listed in Appendix A. This program computes the efficiency and signal-to-baseline (or background) ratio as a function of foil thickness, number of foils, degree of source-resonant material overlay, source and detector recoilless fractions, and detector iron-57 isotopic abundance.

The behavior of the detector efficiency as a function of the various design parameters may best be illustrated by an arbitrary selection of sample calculations shown in the following figures. The principal obstacle to high efficiency is the limited electron range. For 97 percent iron-57 enrichment, the resonant half-value-layer (half-thickness) in  $\text{FeBe}_5$  is  $1,858 \text{ \AA}$ , such that fully half of the "Mössbauer" electrons created in a single foil detector are created at depths greater than this amount. From Figure 11 it is obvious that electrons created at such depths are severely attenuated. We would like to bring the electrons created in the foil as close to the counting surface as possible. This may be done by (1) enriching the foil in iron-57 and thus decreasing the resonant half value layer, or (2) segmenting the foil into several thinner ones so that the total foil thickness traversed by the photon flux is no longer the depth from which the electrons must escape. Since, as we have seen, even 97 percent enrichment is inadequate, a combination of the two methods is necessary. Figure 12(b) shows the improvement as a two half value layer 97 percent enriched foil of two half value layer thickness is subdivided into an increasing number of foils. Since the efficiency is an ever-increasing number of foils, the limitation is a technological one because of the difficulty in fabricating extremely thin layers. In addition, the signal-to-background ratio described below must also be considered.

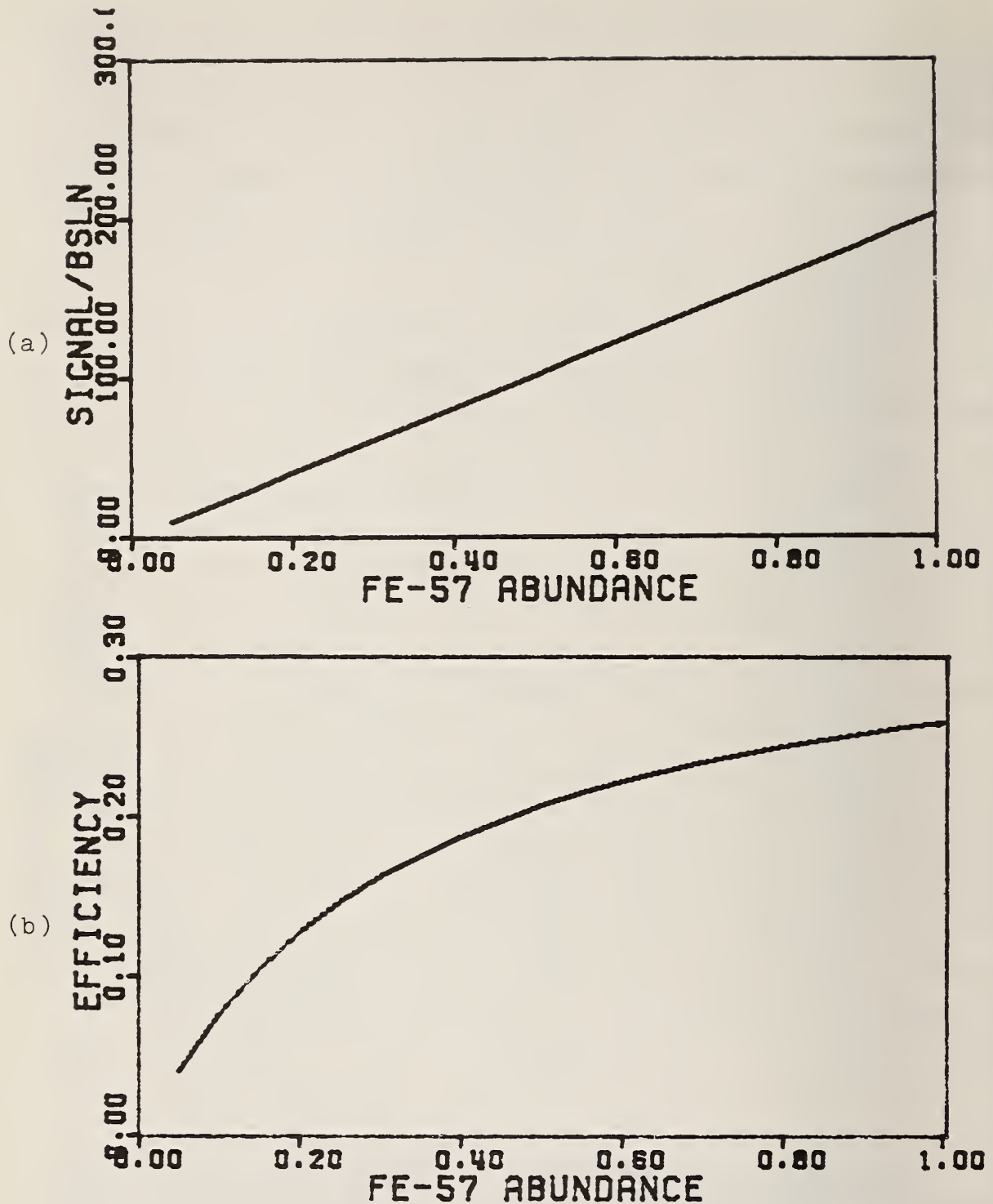
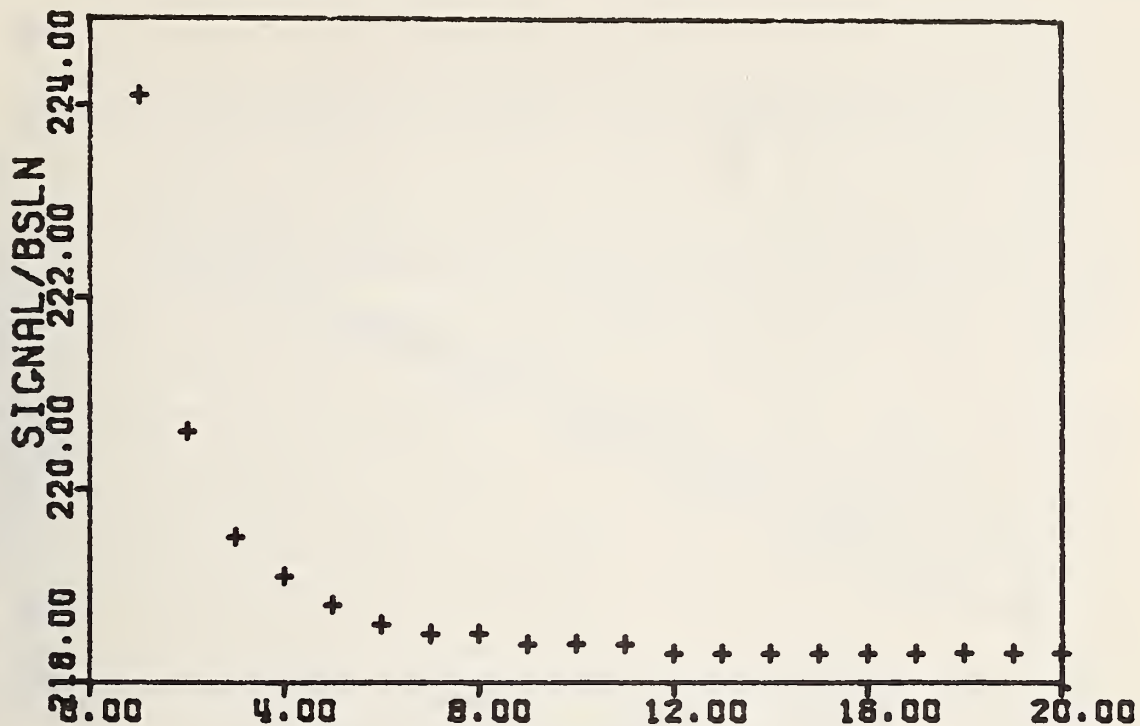


Figure 12. a) Signal-to-baseline (background). b) Detector efficiency as a function of iron-57 abundance for a ten foil detector with a total thickness of two resonant half values, assuming  $f_s = f_D = .95$ .

(a)



(b)

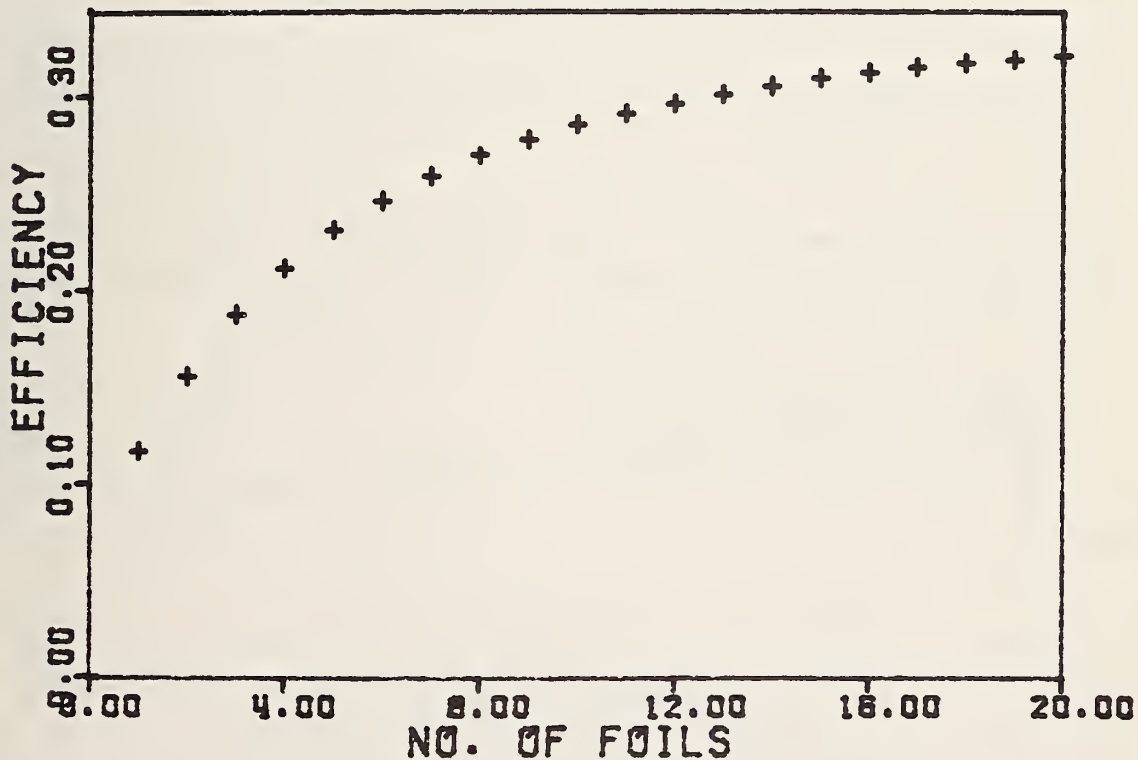


Figure 13. a) Signal-to-baseline (background) ratio.  
b) Detector efficiency as a function of the number of foils for a total thickness of half value layers (3,716 Å) of iron-57 enriched  $\text{FeBe}_5$ .

Figures 14(b), 15, and 16 show studies of the efficiency of 1, 3, 5, and 7 foil detectors for 97 percent, 50 percent, and 3 percent enrichment as a function of total foil thickness. An interesting feature shared by all of these figures is that the efficiency monotonically increases with increasing thickness for a single foil detector, but reaches a maximum at a finite thickness for detectors having more than one foil. For a single foil, the monotonic increase is explained by the fact that more recoilless photons are converted to electrons as the foil thickness is increased; the rate of increase, however, decreases because the additional electrons emitted due to increased thickness are less likely to escape from the foil and be counted. For multi-foil counters, the efficiency initially rises faster with thickness than for the single foil counter because electrons created in the second through the last foils are closer to the surface than they would have been for the same traversed thickness in a single foil. As the thickness increases, however, more and more photons are stopped in the first foil, reducing the opportunity of the succeeding foils to contribute to electron production. Thus, in the limit of infinite thickness, all of the curves must converge to the same limit as the single foil curve, since at infinite thickness, all of the photons are absorbed in the first foil.

#### D. Signal-to-background Ratio

Although the attainment of a high efficiency is important for the most economical source utilization, in principal, the real selling point for the resonant detector, is its ability to respond selectively to the desired radiation. This selectivity can be measured by a signal-to-noise ratio, which we prefer to call a signal-to-background or signal-to-baseline ratio to avoid confusion with the Mössbauer spectroscopist's normal utilization of "noise" as descriptive of the statistical scatter associated with random radiative processes. The ratio of the signal (desired counts) to the background (undesired



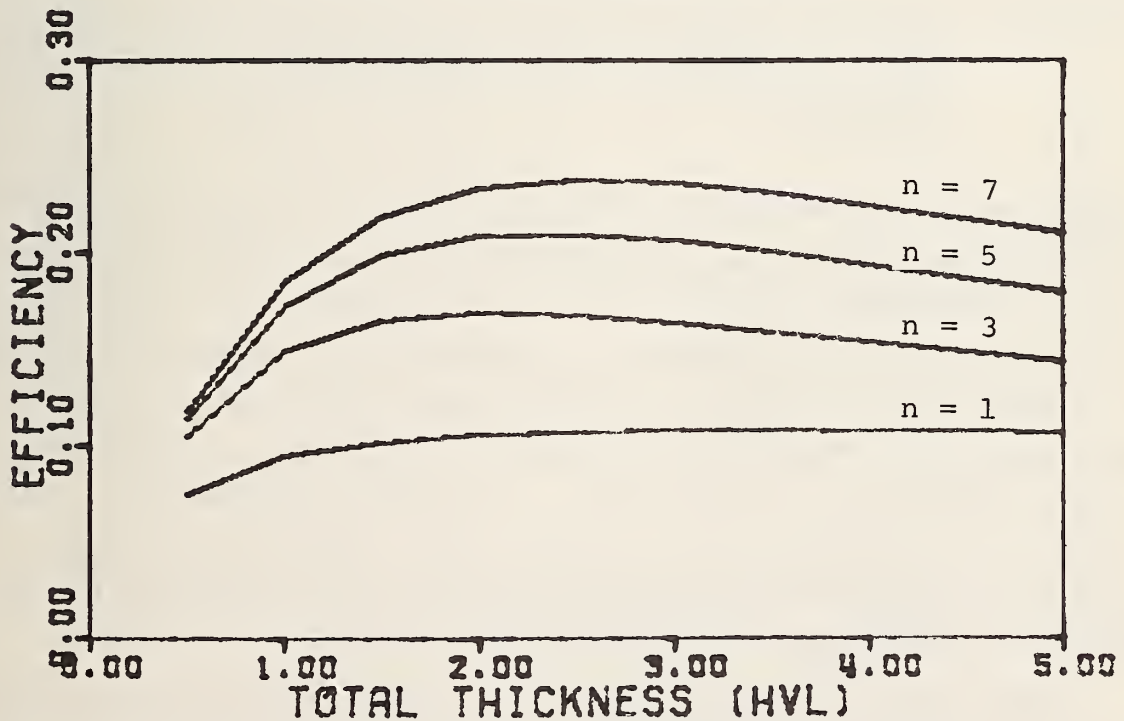
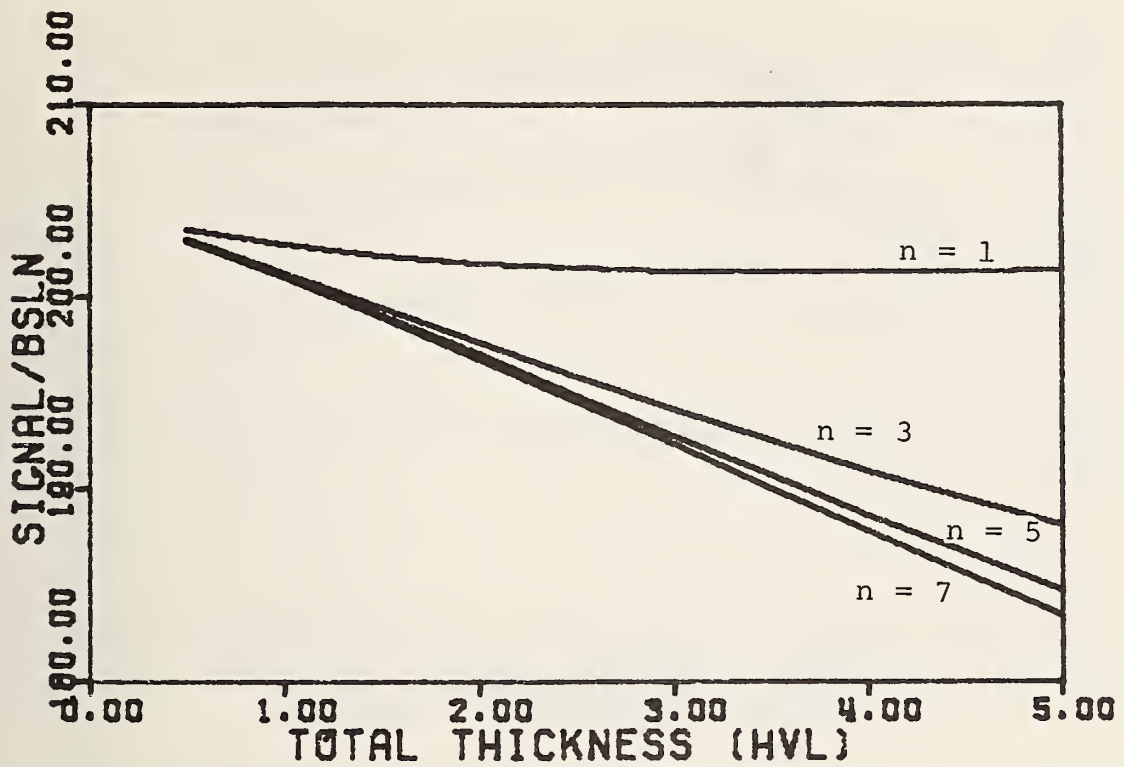


Figure 14. a) Signal-to-baseline (background) ratio. b) Detector efficiency as a function of total thickness of foil(s) for 97 percent iron-57 abundance. One resonant half value layer = 1,858 Å, one photo-electric hvl = 239 resonant hvls. n = number of foils.

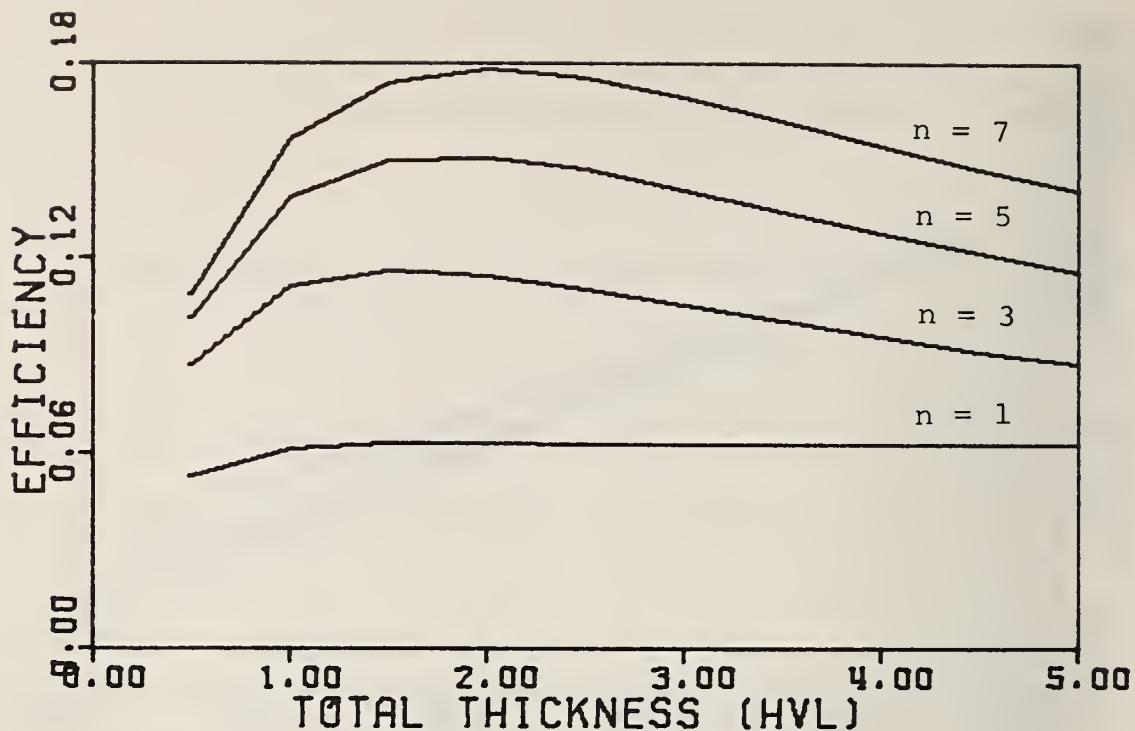


Figure 15. Detector efficiency as a function of total thickness of foil(s) for 50 percent iron-57 abundance. One resonant half value layer (hvl) = 3,604 Å; one photoelectric hvl = 123 resonant hvls. n = number of foils.

counts) may be observed by moving the source relative to the detector, thereby taking a Mössbauer spectrum of the detector, such as that shown in Figure 28. The height of the baseline of the spectrum thus generated represents the background, while the signal is the height of the resonant peak above the baseline, hence the "signal-to-baseline" terminology. Although such spectra of the detector are useful for optimization, they should not be confused with spectra taken with the detector, for which the source and detector remain in resonance (at zero relative velocity).

Figure 12(a) shows the expected signal-to-baseline improvement with increasing iron-57 enrichment. This occurs because the total thickness required to produce a given number of the desired Mössbauer electrons decreases with increasing enrichment, hence the thickness available for producing unwanted

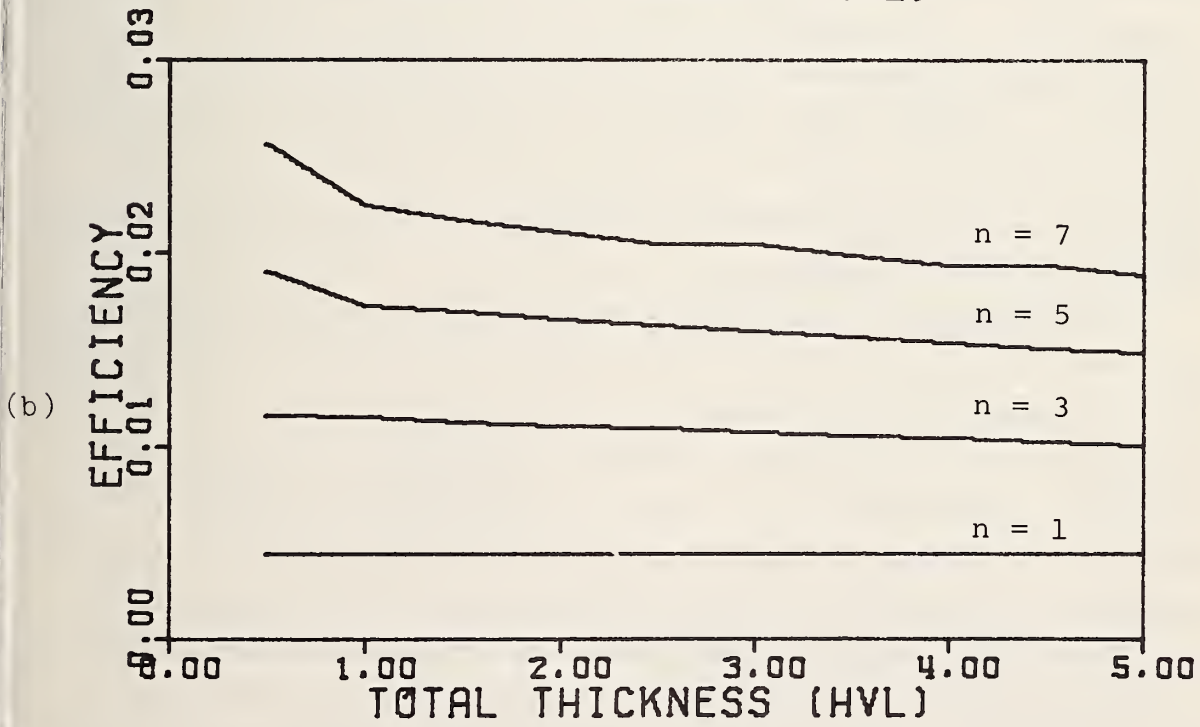
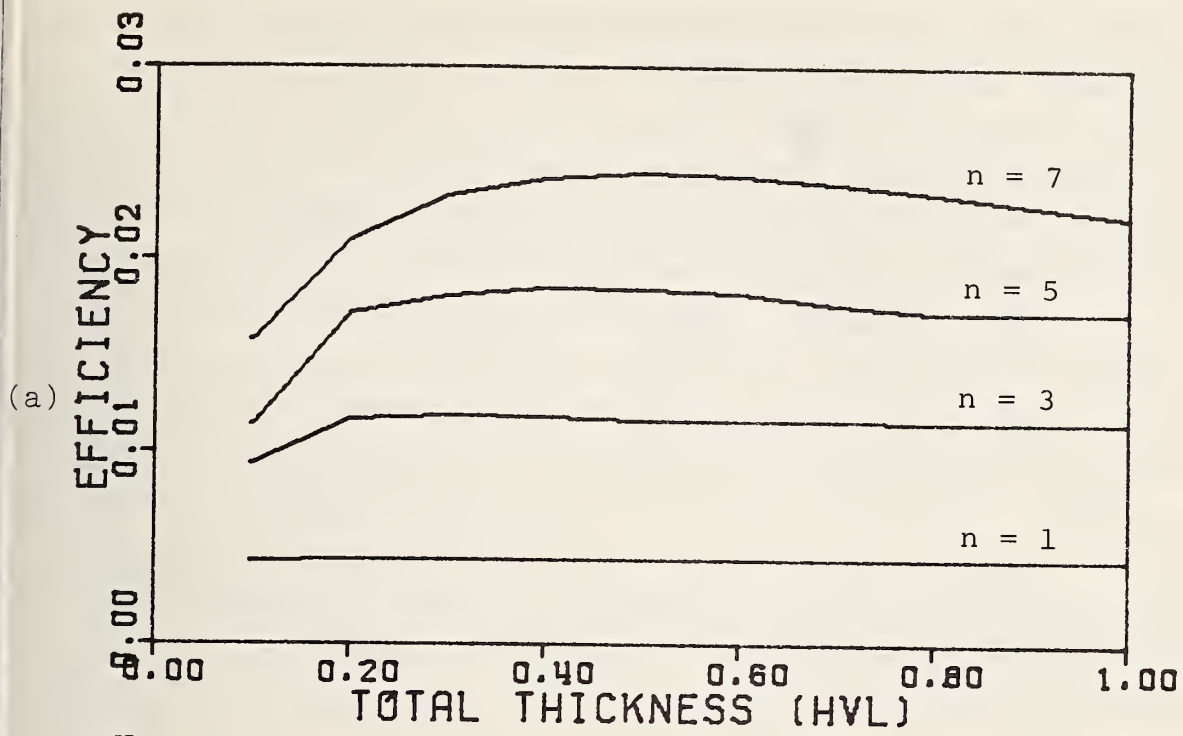


Figure 16. a) and b) Detector efficiency as a function of total thickness of resonant foils, expressed in resonant half value layers, for 3 percent iron-57 abundance. One resonant half value layer = 60,069 Å; one photoelectric hvl = 7.4 resonant hvls. n = number of foils.

photoelectrons may be decreased. When the number of foils is increased, however, the signal-to-baseline ratio decreases with increasing partition of the resonant material, in contrast to the behavior of the efficiency. This behavior relates to the fact mentioned earlier that the proportioning between resonant and nonresonant photons in the beam changes as a function of the thickness traversed. Specifically, resonant photons are removed from the beam at a higher rate than are nonresonant photons so that, as more material is traversed, a higher proportion of unwanted photoelectrons are produced per thickness increment. In other words the "incremental signal-to-background" ratio decreases with increasing photon penetration. The overall ratio is a weighted average of the incremental ratios with the weighting factor being proportional to the detectability of the electrons from a given depth. Thus, for a single foil, the overall ratio is weighted in favor of the shallow depth increments with higher incremental ratios. As the foil is partitioned, electrons produced further along the photon penetration path become more detectable, due to the additional counting surfaces introduced, thereby lowering the overall weighted average.

The signal-to-baseline ratio as a function of total thickness for 97 percent iron-57 enrichment is shown in Figure 14(a). The convergence of the curves for different numbers of foils in the thin limit is expected because the change in resonant proportion discussed above requires a finite thickness to be effective. Because of the linearity of signal-to-baseline with enrichment, as shown in Figure 12(a), the relationship shown in Figure 14(a) may be reproduced for other enrichment factors by applying the enrichment ratio to the signal-to-baseline axis of 14(a). For instance, for 50 percent abundance, the numbers on the signal-to-baseline axis of 14(a) should be multiplied by 50/97.

The signal-to-baseline and efficiency values resulting from these computations are far greater than any observed

experimentally to date. This is due partly to the fact that enrichment and thin film production is less expensive and more easily done theoretically than experimentally. However, there are undoubtedly additional errors resulting from the simplifying assumptions regarding the production of "noise" electrons in the foils), the neglect of electron "straggling" effects, lack of consideration of noise production in the counting gas and counter walls, and others. The final optimization process must certainly be experimental, but these computations, and future ones, should provide useful guidelines despite these deficiencies.

#### E. Line Width

The line profile  $L(v, \Gamma)$  observed in Mössbauer spectroscopy is the convolution of the source  $L_S(v_S, \Gamma_S)$  and the absorber  $L_A(v_A, \Gamma_A)$  profiles, or

$$L(v_S - v_A, \Gamma) = \int_{-\infty}^{\infty} L_S(v_S, \Gamma_S) \cdot L_A(v_S - v_A, \Gamma_A) dv_A \quad (11)$$

where  $\Gamma, \Gamma_S, \Gamma_A$  are the half-widths at half-maximum intensity for the observed, source, and absorber line profiles. The source and absorber profiles can be expressed by the Lorentzian function,

$$L(v_o, \Gamma) = \frac{L_o}{1 + \left(\frac{v-v_o}{\Gamma}\right)^2} \quad (12)$$

In the case of a thick absorber, the linewidth is increased due to absorption broadening. Successive layers of material in the absorber will preferentially absorb the radiation in the center of the profile with respect to the wings. The line broadening can be calculated as a function of absorber thickness from the approximate relation,

$$\Gamma_{\text{obs}} = \Gamma_o (2.00 + 0.27t_A) \quad \text{for } t_A < 5 \quad (13)$$

with the absorber thickness  $t_A = f_A n k \sigma_0 t$ , where  $f_A$  is the fraction of the recoil-free radiation,  $kn$  is the number of Mössbauer nuclei per unit area, and  $\sigma_0$  the resonance cross section.

For the resonant detector, the line profile is now a function of the source, absorber, and detector line profiles, which can be calculated from the convolution integral

$$L_R[(v_S, v_D) - v_A, \Gamma_R] = \quad (14)$$

$$\int_{-\infty}^{\infty} L_S(v_S, \Gamma_S) \cdot L_A(v_S - v_A, \Gamma_A) \cdot L_D(v_D, \Gamma_D) dv_A$$

where  $\Gamma_D$  is the detector half-width. The selectivity of the detector reduces the observed half-width, as shown in Figure 17, for the case where  $\Gamma_S, \Gamma_A, \Gamma_D = 1$  and  $v_S = v_D$ . The line profile was obtained by numerical integration, using a computer. A

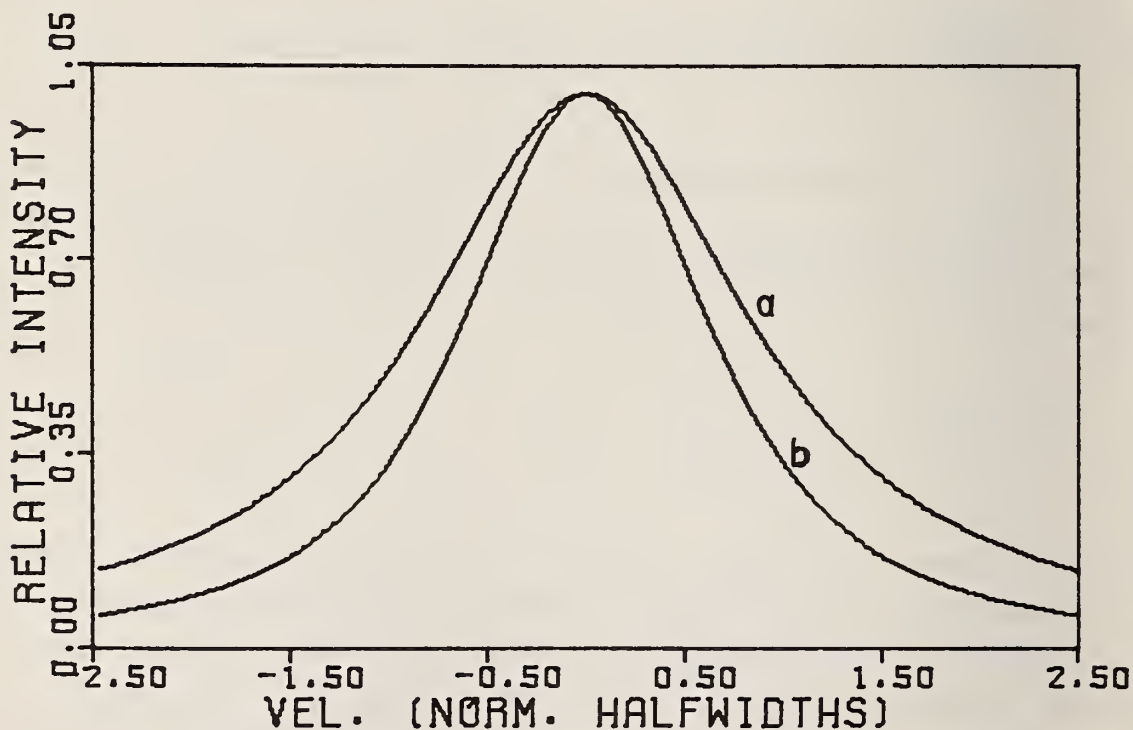


Figure 17. a) Line profile for source and absorber using a conventional detector. b) Line profile for a moving absorber placed between a stationary source and resonant detector.

computer program for this convolution written in BASIC is listed in Appendix B.

For the case of the resonant detector, the thickness broadening can be calculated from the line profile obtained by numerical integration, as was performed by Mitrofanov et al. [8]. They derived an analytical expression for the thickness broadening, given by

$$\Gamma_R = \Gamma_O (1.47 + 0.27t_A) \quad \text{for } t_A < 5 \quad (15)$$

For a thin absorber a 26 percent reduction in linewidth is obtained, which increases the resolution of the spectrometer. Conversely, the resonant detector makes it possible to use much thicker samples without loss of resolution beyond that of the conventional detector, thereby increasing the effect. This will result in a considerable decrease in data accumulation time.

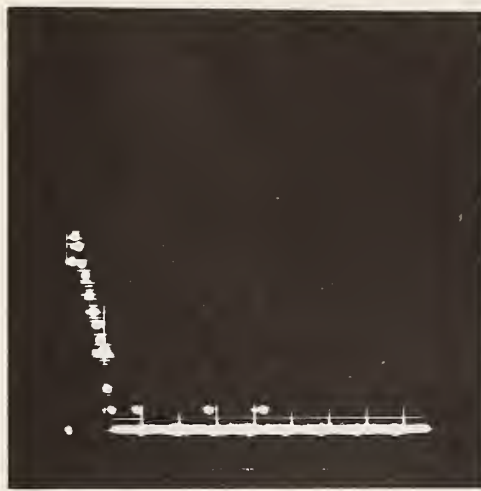
#### 4. PRELIMINARY MEASUREMENTS

Several preliminary measurements were made to obtain data on the efficiency and signal/noise ratio for the different detection methods and types of detectors available. Although the internal conversion process provides the possibility of using either conversion x-ray or conversion electron detection, the x-ray fluorescence and low yield of conversion x-rays due to secondary processes makes the conversion electron detection more efficient. There are several types of detectors available for low energy electron detection, and their inherent noise and sensitivity to x- or gamma-ray radiation will be a decisive factor in the selection of the proper counter. Since the inherent thickness of the conversion material will degrade the energy of the initial conversion electron, the energy resolution of the detector will not be critical. Fast response time for the required high counting rates will be essential. These requirements favor the proportional, electron multiplier, and scintillation detectors, but place the solid state detectors at a disadvantage.

##### A. Resonant Detector for $^{119}\text{Sn}$ Using the Gel Scintillation Technique

The internal conversion factor of 5.5 and the 19.6 keV energy of the conversion electron made  $^{119}\text{Sn}$  a logical choice. Furthermore the gel scintillation technique is well developed and simple to use. The resonant material in finely powdered form is mixed with a scintillation gel and placed on a photomultiplier tube. The gel was prepared from 10 g of PPO (2,5 Diphenyloxazole) and 0.6 g of Dimethyl POPOP (1,4-bis-2-(4-Methyl-5-Phenyloxazolyl)-benzene), which was mixed with enough toluene to yield 2 liters of solution. Calibration of the pulse-height spectrum was made by using a tritium loaded gel. Tritiated glucose, 10.7 mg was mixed with 1.0 ml of  $\text{H}_2\text{O}$  and added to 10 ml of scintillator solution. Various amounts of Cabosil (trade name for silica gel) were then added to this





18.1 keV

Figure 18. Pulse-height spectrum of tritium loaded gel. Endpoint is at 18.1 keV.

solution to obtain the proper gel viscosity. Counting efficiency was the highest for the rigid gel. The pulse height spectrum for the tritium loaded gel is shown in Figure 18. The endpoint energy of the beta-decay is 18.1 keV, which provides a calibration point. For the resonant detector experiments, the gel was made by dispersing finely powdered  $^{119}\text{SnO}_2$  in Cabosil and scintillator solution. The Mössbauer spectrum of a moving  $\text{Pd}_3^{119\text{m}}\text{Sn}$  source and the enriched  $\text{SnO}_2$  absorber-gel is shown in Figure 19. The results were very unsatisfactory due to the large baseline count and the low effect. Most of the baseline counts observed were due to photomultiplier noise, since the pulse height spectrum shown in Figure 20 did not change appreciably when the source was present or not. The early measurements were made with an EMI 6097S tube. Replacing this tube with a RCA C3100 photomultiplier with much less dark current gave very little improvement. It was observed that the photomultiplier tube itself is very sensitive to gamma-radiation, due to photoelectrons being produced in the envelope and photocathode. In order to eliminate the direct gamma radiation from the photomultiplier and also to reduce the tube noise,

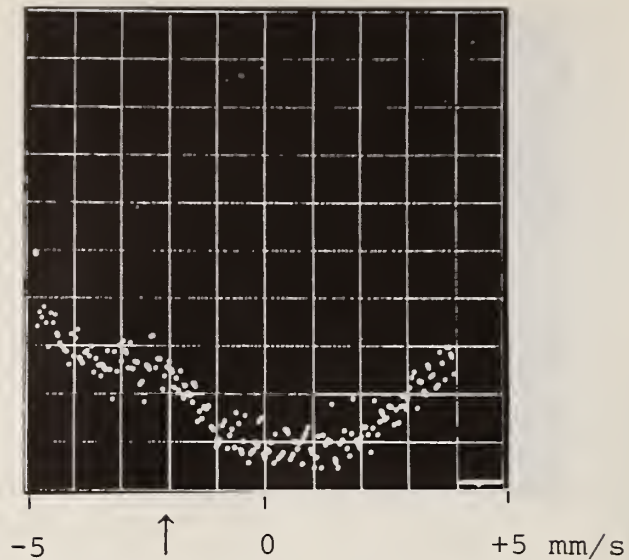


Figure 19. Mössbauer spectrum of  $^{119}\text{SnO}_2$  dispersed in scintillation gel and moving  $\text{Pd}_3^{119\text{m}}\text{Sn}$  source. Peak is barely visible at  $-2.2 \text{ mm/s}$ .

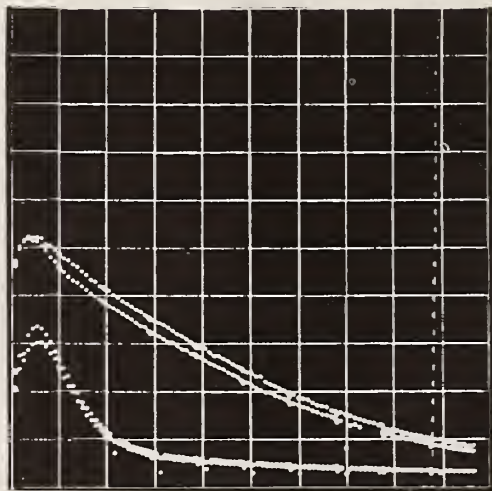


Figure 20. Pulse-height spectrum of gel scintillation counter. Upper spectra: H.V. = 2000 volts, upper curve with, lower curve without source. Lower spectra: same, but H.V. = 1200 volts.

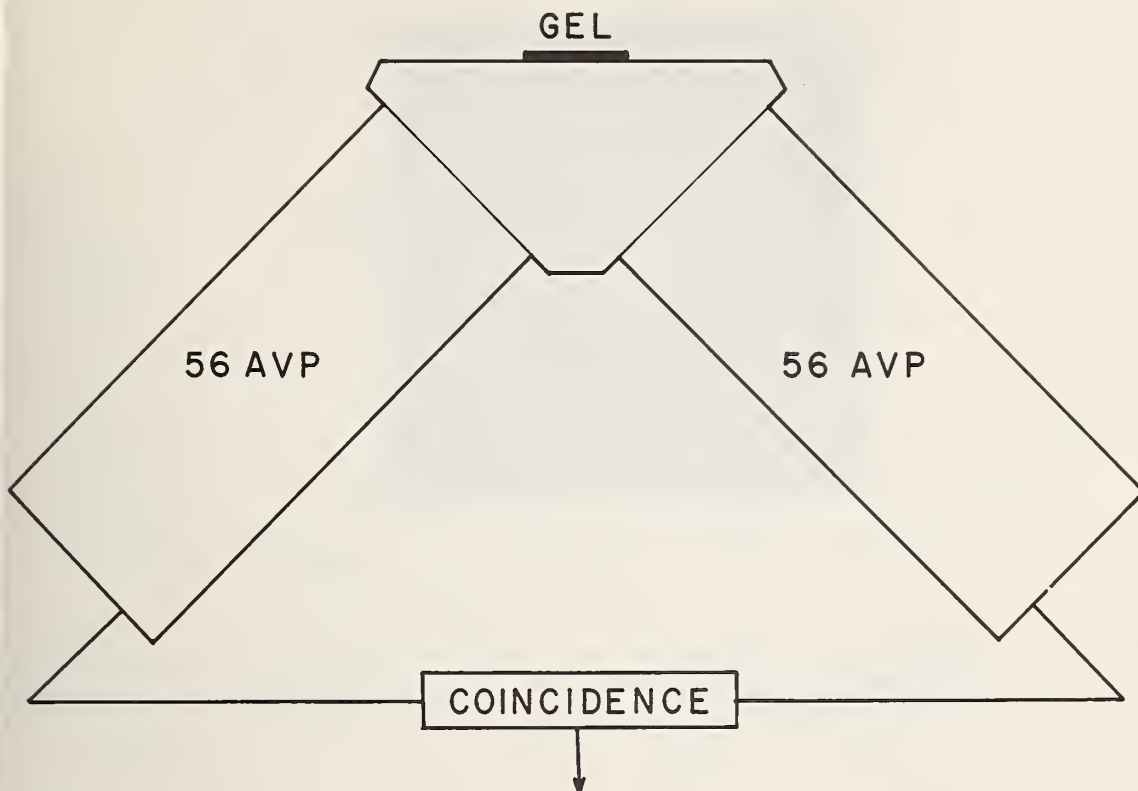


Figure 21. Coincidence arrangement for gel scintillation detector. Photomultiplier tubes are shielded from direct gamma radiation.

two Amperex AVP 53 tubes were placed in coincidence, and connected by a light pipe to the gel sample. See Figure 21. The AVP 53 tubes were selected because of their fast rise time, which is required for high counting rates. The Mössbauer spectra obtained with this arrangement is shown in Figure 22. The results are poor, and confirmed the measurements made by [5].

The energy of the conversion electron from  $^{119}\text{Sn}$  is very close to the detection limit of present scintillation systems. Furthermore, the energy degradation in a solid such as  $\text{SnO}_2$  is large, which will lower the energy of the conversion electron escaping the  $\text{SnO}_2$  particle. The use of a tin compound soluble in the scintillator solution would help the finite particle problem, but all Mössbauer data on organo-tin compounds show

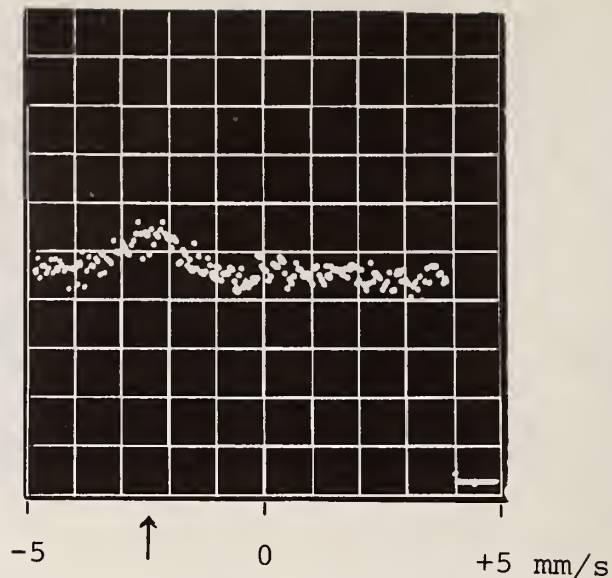


Figure 22. Mössbauer spectrum of  $^{119}\text{SnO}_2$  dispersed in scintillation gel and  $\text{Pd}_3^{119\text{m}}\text{Sn}$  source, using coincidence noise suppression.

a very small effect (low  $f$ -factor), whereas a resonant detector requires a very high  $f$ -factor.

The scintillation process is very inefficient. Electrons interact with the scintillator, producing  $3000 \text{ \AA}$  wavelength photons, which interact with the photocathode to produce a very low energy electron, which is then used in the multiplication process.

B. Resonant Detector for  $^{57}\text{Fe}$  Using a Conversion Electron Proportional Counter.

The background noise in the gel scintillation technique and the lower energy (7.3 keV) for the conversion electrons in  $^{57}\text{Fe}$  made this technique very unattractive for iron Mössbauer spectroscopy. However, He filled proportional counters have a low background, are rather insensitive to x-ray radiation and are very efficient in detecting low energy electrons. To optimize the geometrical efficiency a flat proportional counter was designed.

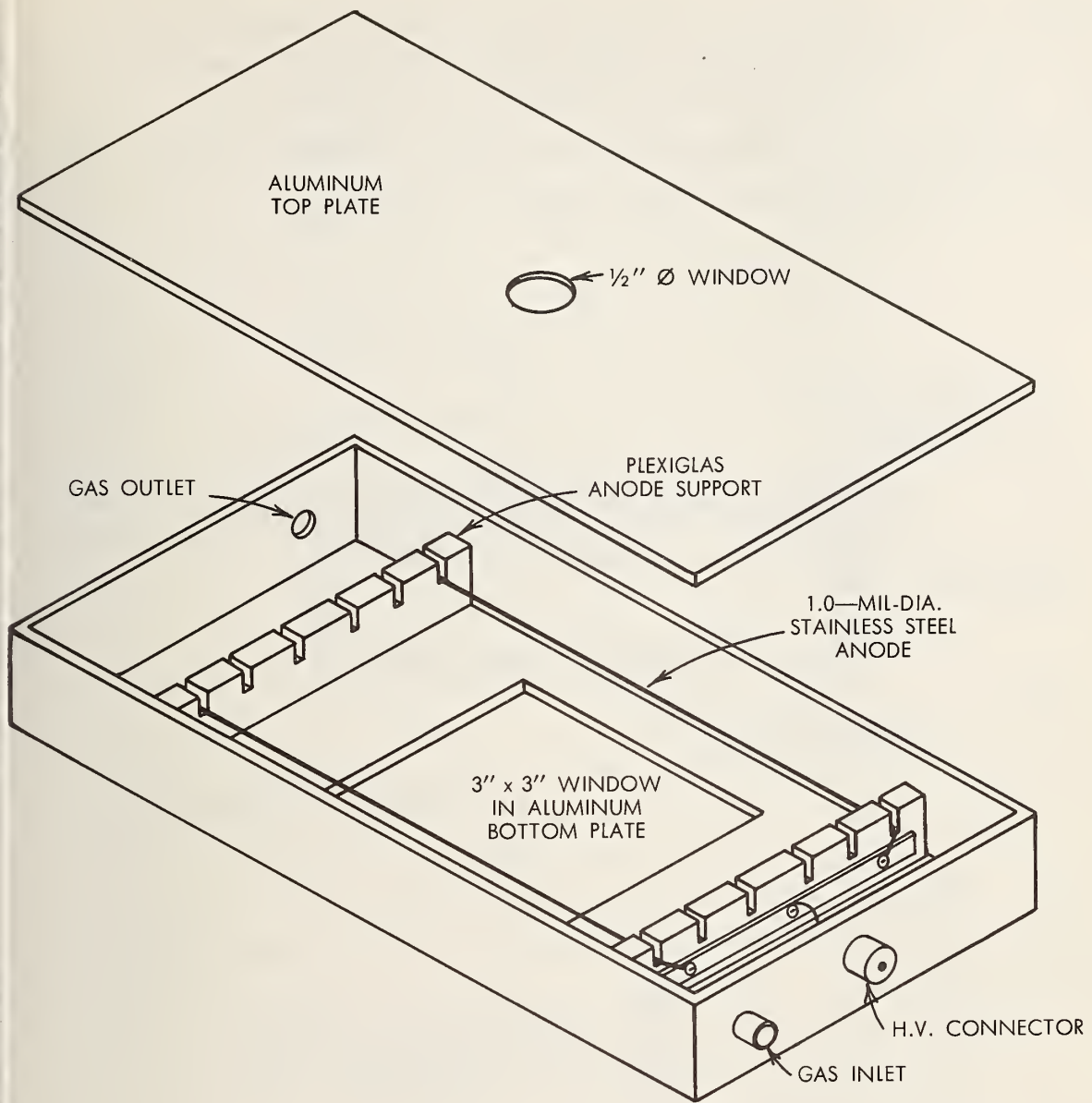
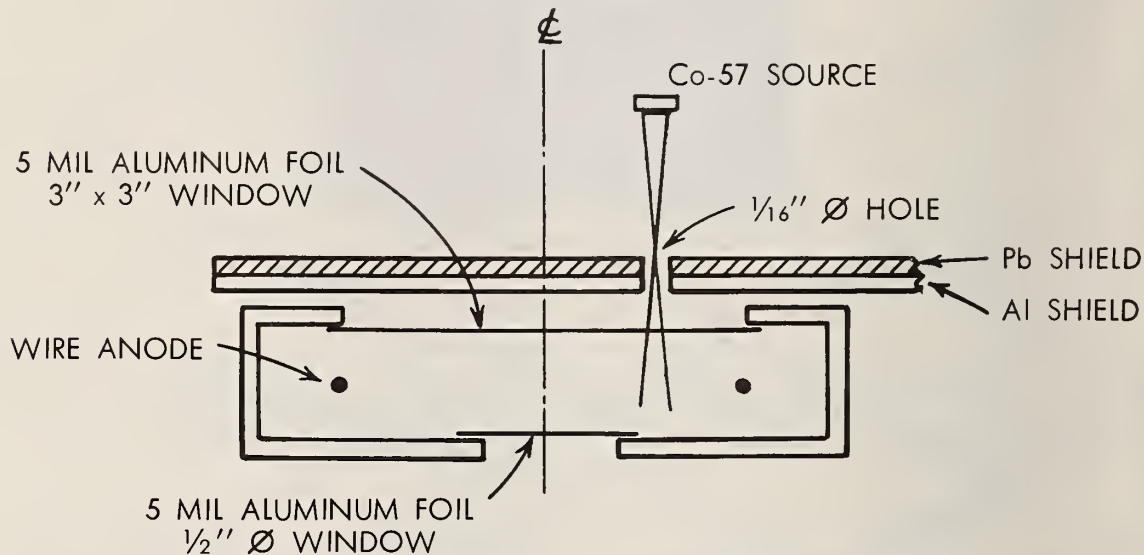


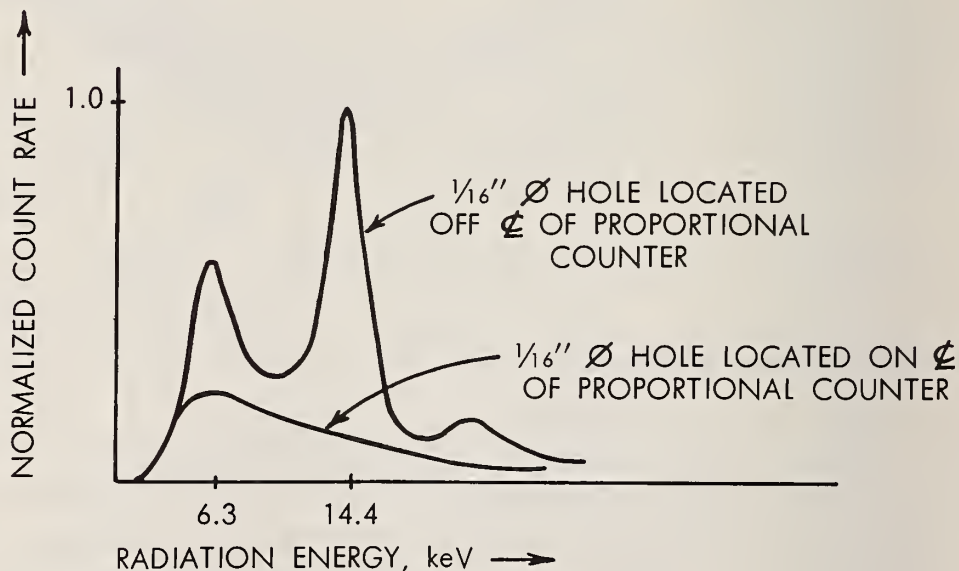
Figure 23. Isometric view of proportional counter with top plate removed.

As shown in Figure 23, the proportional counter is rectangular in appearance with removable top and bottom plates to facilitate rearrangement of the wire anodes as desired. The anode configuration used in this work consisted of two one-mil-diameter stainless steel wires spaced three inches apart. During operation of the counter, the anodes were kept at approximately 1400 V with respect to the grounded aluminum shell. The

counter has two windows. One is 1/2 inch in diameter and the other is 3 inch x 3 inch square. The choice of window covering and flow gas varied somewhat, as will be noted later. After an initial purge to remove air from the counter, the gas flow rate was maintained at approximately  $1 \text{ cm}^3/\text{s}$ .



(a) EXPERIMENTAL ARRANGEMENT



(b) PULSE-HEIGHT SPECTRA

Figure 24. Pulse-height spectra for Co-57 Mössbauer source as a function of position on 3 inch x 3 inch window.

The arrangement shown in Figure 24a was employed to obtain pulse-height spectra of the radiation from a cobalt-57 Mössbauer source as different locations on the 3 inch x 3 inch window were irradiated. Both proportional counter windows were covered with 5-mil-thick aluminum foil. An argon-10 percent methane flow-gas was used. A lead-and-aluminum shield with a 1/16 inch-diameter hole restricted the radiation to the desired area of the window. The pulse-height spectra obtained at all points on the 3 inch x 3 inch window were virtually identical in terms of resolution, counting efficiency, and gas multiplication, except for those pulse-height spectra taken at points along the counter centerline midway between the two wire anodes. The efficiency of the counter at these points was decreased by approximately a factor of two for the 6.3 keV x-ray; furthermore, the 14.4 keV gamma ray was practically undetected. A comparison of the two types of pulse-height spectra are shown in Figure 24b. As little as 0.2 in deviation from the centerline of the counter resulted in the full pulse-height spectrum illustrated by the upper curve in Figure 24b. This characteristic of low detection efficiency at the center of the counter results in an improved signal-to-noise ratio for backscatter measurements when the collimated incident radiation is directed through the center of the counter where it is less likely to contribute to the background. Typical Mössbauer spectra taken with this counter are shown in Figure 7. The area of the described counter is too large for a resonant detector. A smaller counter, with a 0.5 inch diameter aperture and 0.25 inch thick was designed, as shown in Figures 25 and 26, and the two 1 mil wires were spaced for optimum efficiency and resolution. This counter operates at 1200 V, using a He-8 percent CH<sub>4</sub> flow gas. The energy calibration of the detector was determined by placing a <sup>55</sup>Fe source in the counter, which gave the typical spectrum with a 5.5 keV endpoint for <sup>55</sup>Fe and a 7.3 keV endpoint for a <sup>57</sup>Co source, shown in Figure 27. To evaluate this counter for a resonant detector, a commercial 0.5 mil 50

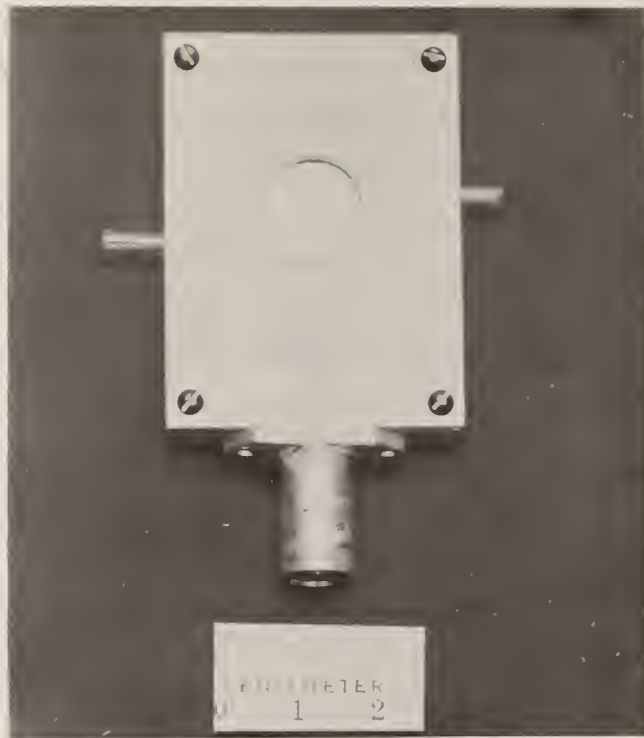


Figure 25. Photograph of detector for conversion electrons.

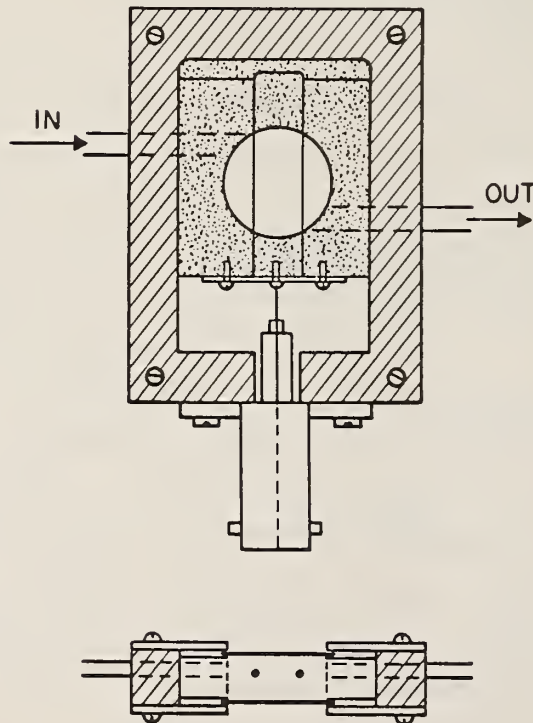


Figure 26. Diagram of detector for conversion electrons.



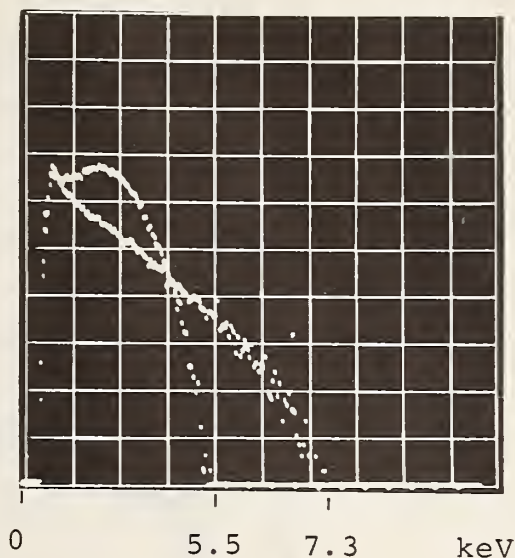


Figure 27. Pulse-height spectra of a  $^{55}\text{Fe}$  (5.5 keV endpoint) and  $^{57}\text{Co}$  (7.3 keV endpoint) source placed inside the detector.

percent enriched stainless steel foil was placed inside the counter over the exit window. The spectrum of a moving  $^{57}\text{Co}$  in stainless steel source with this detector is shown in Figure 28. The signal/background is 325 percent. The energy dependence of the background electrons, Figure 29a, was obtained by taking a pulse height spectrum with the source scanning at high velocity. Figure 29b shows the electron spectrum with the source at rest, which corresponds to the sum of the background and resonantly generated electrons. Both spectra show a large energy dependence, and for optimal signal/background, pulse-height selection will be required. The energy dependence of the conversion electrons, obtained by subtracting the spectra of 29a and b is shown in Figure 30. The differential signal/noise shown in Figure 31 can be used for optimum energy selection by proper setting of the single channel analyzer. The performance of this detector agrees well with the theoretical analyses made in Section 2, for a resonant detector made with a single thick foil.

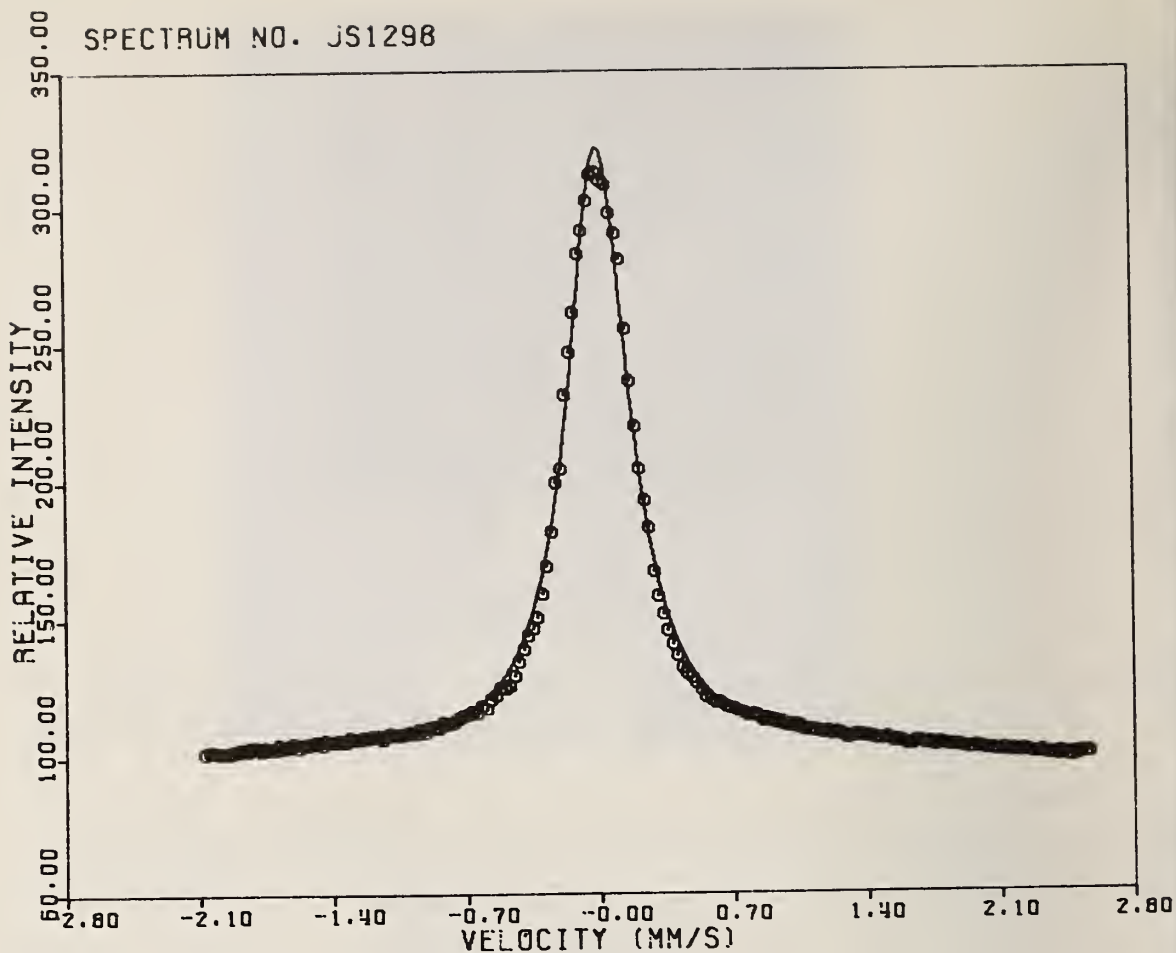


Figure 28. Mössbauer spectrum of the resonance detector with a 0.5 mil 50 percent enriched stainless steel foil and moving  $^{57}\text{Co}$  in stainless steel source.

The use of a stainless steel converter material is far from optimum. The 18 percent Co and 8 percent Ni content in this alloy increases the photoelectron contribution and attenuates the Mössbauer gamma radiation. Thin foils of this material are also difficult to fabricate. The theoretical analyses showed that a low Z element for alloying to collapse the magnetic field in iron is very important, and beryllium would be the best material available. Fe-Be alloys near the composition  $\text{Be}_5\text{Fe}$  were found to be nonmagnetic and exhibited a narrow Mössbauer spectrum, with a large resonant effect. The alloy composition, thickness of the foils and number of foils

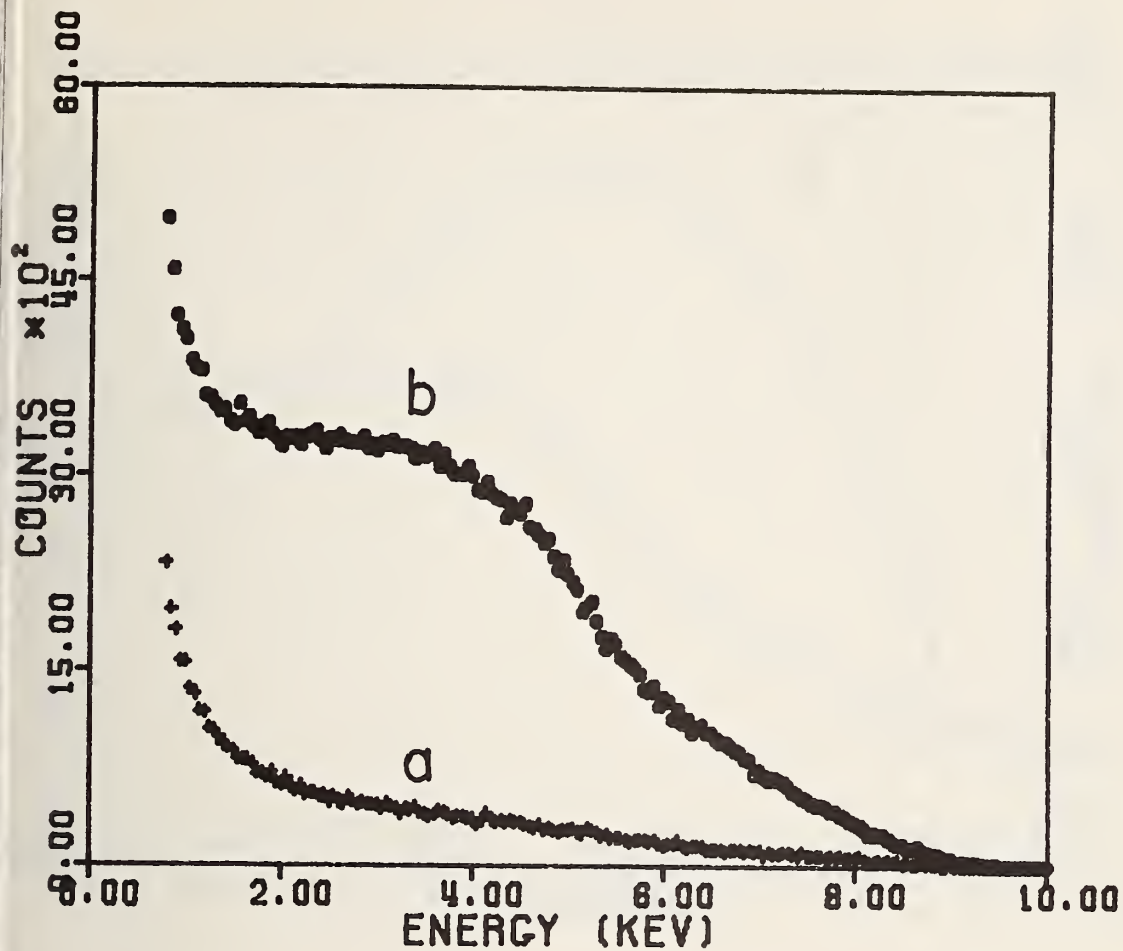


Figure 29. Energy distribution of photoelectrons and conversion electrons obtained by source-detector off resonance (a) and in resonance (b).

required and the final construction and fabrication of the counter will be the basis of the second report (FY1970) on this investigation.

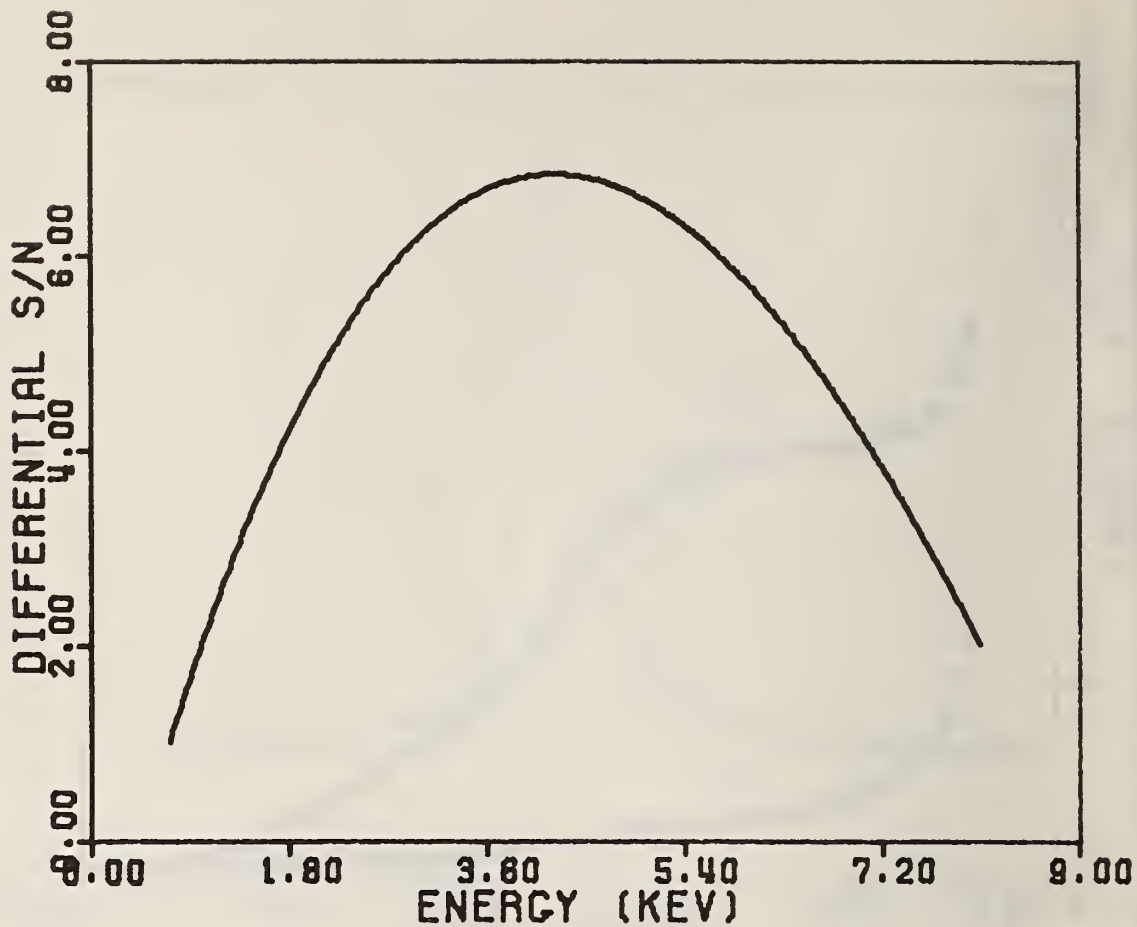


Figure 30. Energy distribution of the conversion electrons from a 0.5 mil 50 percent enriched stainless steel foil.

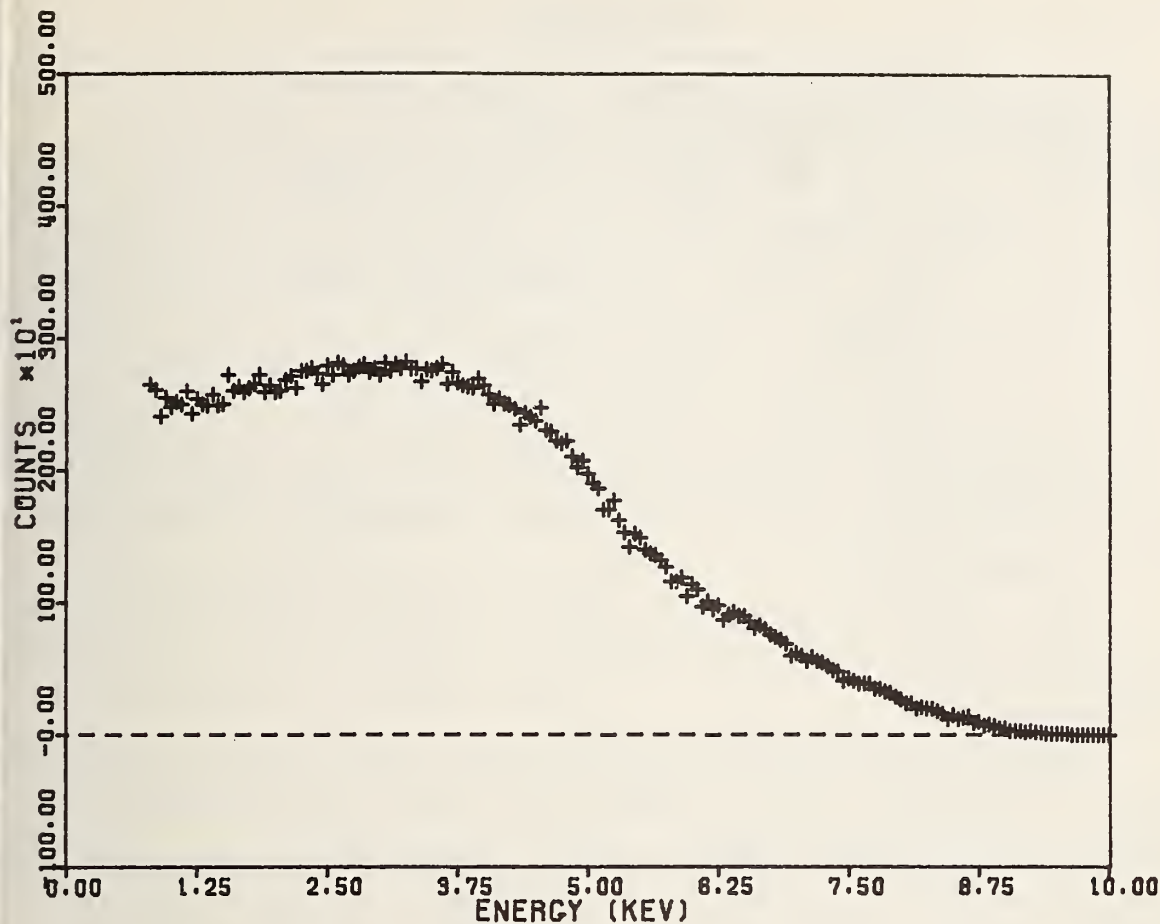


Figure 31. Differential signal/noise of the electrons generated in the stainless steel resonant detector. Optimum selection would be from 2 to 6 keV.

## 5. SUMMARY

It is apparent that there are many advantages in using the resonant detector for Mössbauer spectroscopy. Because the detector is so selective for the Mössbauer radiation it can be used to great advantage where the background (non-resonant) radiation is high. This is the case with samples exhibiting low Mössbauer effect or from a close scattering geometry or when a very small amount of material is available to be measured such as particulate matter on a substrate of filter paper. In addition, this detector will prove to be very valuable in the Mössbauer spectroscopy of complex materials because of its high resolution.

The same detector system can be used to measure the structure of surface films on bulk material that is less than 200 Å in thickness.

Because the resonant detector is so selective the combination of increased source strength with the optimal number and thickness of resonant material will significantly decrease the collection time for a spectrum of a given quality. Evaluation of the various detector systems described in this report will be made by quantitative experimentation.

## 6. REFERENCES

- [1] Mitrofanov, K. P., Illarinova, N. V. and Shpinel, V. S. Proceedings of the Dubna Conference on the Mössbauer Effect, Consultants Bureau Enterprises, Inc., New York, (1963). Translation from Russian.
- [2] Mitrofanov, K. P. and Shpinel, V. S., Zhur. Eksp. i Teoret. Fiz., 40 983 (1961).
- [3] Mitrofanov, K. P., Illarinova, N. V., Shpinel, V. S., Prit. Tekh. Eksper. N3, 49 (1963).
- [4] Aleksandrov, A. Yu., Kerasev, A. N., Mitrofanov, K. P., Sorokin, A. A. and Polak, L. S., Coll: Problems of Nuclear Geophysics (in Russian) Izd. "NEDRA" (1964).
- [5] Levy, L., Mitrani, L., Ormandjiev, S., Nucl. Instr. Methods 31, 233-6 (1964).
- [6] Bonchev, ZW, Jordanov, A., and Minkova, A., Nucl. Instr. Methods 70, 36-40 (1969).
- [7] Mitrofanov, K. P., Instruments and Experimental Techniques, (PTE), No. 3 60 (1965).
- [8] Mitrofanov, K. P., Plotnikova, M. V., and Rokhlov, Instruments and Experimental Techniques, (PTE), No. 4, 790 (1965).
- [9] Mirtofanov, K. P., and Rikhlov, N. I., Instruments and Experimental Techniques, (PTE) No. 5, 1256 (1965).
- [10] Shimony, U., Nucl. Instr. Methods, 37, 350 (1965).
- [11] Protop, C. and Nistor, C., Rev. Roum. Phys., 12, 658 (1967).
- [12] Chow, H. K., Weise, R. F., Flinn, P., "Mössbauer Effect Spectrometry for Analysis of Iron Compounds", AEC Rept. NSEC-4023-1 TID-4500, Contract No. At-(30-1)-4023 (1969).
- [13] Ord, R. N., Appl. Phys. Letters, 15, 279 (1969).
- [14] Terrell, J. H. and Spijkerman, J. J., Appl. Phys. Letters 13, 11 (1968).

- [15] Swanson, K. R. and Spijkerman, J. J., June 1970.  
DeVoe, J. R., Editor, NBS Technical Note 501, Superintendent of Documents, U. S. Government Printing Office Washington, D. C., 20402 (1970).
- [16] Muray, J. J., Worster, B. W., IEEE Transaction on Nuclear Science, Vol. NS-14, No. 4, 11-16 (1967).
- [17] Berthelot, André, Radiations and Matter, Leonard Hill [Books] Limited, London (1958).
- [18] Cosslet, V. E. and Thomas, R. N., Brit. J. Appl. Phys., 15, 883-907 (1964).
- [19] Spijkerman, J. J., Snediker, D. K., Ruegg, F. C. and DeVoe, J. R., NBS Misc. Publ. 260-13, Superintendent of Documents, U. S. Government Printing Office, Washington, D. C., 20402 (1967).



APPENDIX A: TO COMPUTE RESONANT DETECTOR EFFICIENCY AND  
SIGNAL BACKGROUND RATIO AS A FUNCTION OF  
ASSORTED INPUT PARAMETERS

```

1 REM PROGRAM /SELEC/ TO COMPUTE RESONANT DETECTOR EFFICIENCY AND
2 REM SIGNAL/BACKGROUND RATIO AS A FUNCTION OF ASSORTED INPUT
  PARAMETERS.
9 OPEN 4,OUTPUT,/ATTN2/
10 OPEN 3,OUTPUT,/ATTEN/
11:#####!!!! #####!!!!
12:#####.
25 DIM U(50),V(50,3),T(2),R(2),E(2)
30 REM A=IC COEF; I4,I2,I6=14.4,122,136 KEV TRANSITION PROBS.
35 REM CONVERTED TO INCIDENT INTENSITIES
41 V9=0
42 V8=0
45 READ A,I4,I2,I6
49 I4=I4/(1+A)
50 FOR J=1 TO 3
51 FOR I=1 TO 50
52 V(I,J)=0.
53 NEXT I
54 NEXT J
55 REM F1=SOURCE FRACTION,F2=DETECTOR FRACTION,A1=DETECTOR
  ISOTOPIC
60 REM ABUNDANCE, D5=SOURCE-DETECTOR OFFSET, G1=SOURCE HW,G2=DET.
  HW
65 REM S0=RESONANT X-SECTION,M0=RES. LINEAR ATTEN. COEF.
70 REM S1= 14.4 FE PHOTO X-SECTION, M1=CORRESPONDING LIN. ATTEN.
  COEF.
75 READ F1,F2,A1,D5,G1,G2
80 S0=2.2E-18*A1*F2/(1.+(D5/(G1+G2))^2)
85 REM R1=FE-BE-5 DENSITY, N1=#IRON/CC,N2=#BE/CC,T2=HALF VALUE
  LAYER
90 READ R1,N1,N2,S1
95 M0=N1*S0*10.^-8
96 M1=N1*S1*10.^-8
97 T(2)=.693/M1
98 T(1)=.693/M0
99 PRINT "RESONANT HALF VALUE LAYER=";T(1);"ANGSTRØMS"
100 PRINT "NON-RESONANT HALF VALUE LAYER=";T(2);"ANGSTRØMS"
103 PRINT "CONVERSION ELECTRON RANGE=8735 ANGSTRØMS"
104 PRINT "AUGER ELECTRON RANGE=5807 ANGSTRØMS"
105 PRINT "FOIL THICKNESS, ANGSTRØMS:";
110 INPUT T1
115 N3=T(1)/T1
116 D8=T(1)/10.
120 PRINT N3;"FOILS PER RESONANT HALF VALUE LAYER"
125 PRINT "NUMBER OF FOILS:";
130 INPUT N4
135 F3=N4*T1/T(1)
140 PRINT "TOTAL THICKNESS=";F3;" HALF-VALUE LAYERS"
145 REM E=ELECTRON ENERGY, R=RANGE,E1=ELECTRON EXIT ENERGY

```

```

150 READ E(1),E(2),R(1),R(2)
151 DEF FNA(X)=R(1)*X*LØG(R(1)/X)/(R(1)-X)
152 DEF FNB(X)=R(2)*X*LØG(R(2)/X)/(R(2)-X)
153 DEF FNC(X)=.991/(1.+((3.205-X)/36.76)+2)
154 DEF FND(X)=1.01/(1.+((-6.7-x)/66.86)+2)
155 REM Q1=RESØNANT PHØTØNS REACHING GIVEN DEPTH
160 REM Q2=TØTAL PHØTØNS REACHING GIVEN DEPTH
165 REM P1=NØ. MØSSBAUER IC ELECTRØNS CREATED AT GIVEN DEPTH
170 REM .7*P1=NØ. MØSSBAUER AUGER ELECTRØNS (ETC.)
175 REM P2=NØ. PHØTØELECTRIC K ELECTRØNS CREATED
176 REM .7*P2=NØ. PHØTØELECTRIC AUGER ELECTRØNS
180 Q1=F1*I4
185 Q2=I4
194 D=R(1)/10
195 IF R(1)<T1 THEN 198
196 D=T1/10
198 FØR K=1 TØ N4
200 D1=D/2
205 REM D=DEPTH INCREMENT, D1=DEPTH
210 P1=Q1*MØ*D
215 P2=Q2*M1*D
220 Q1=Q1-P1-P2*(Q1/Q2)
225 Q2=Q2-P1-P2
226 IF D1>R(1) THEN 340
227 D2=D1*R1/100.
228 D3=FNA(D1)*R1/100.
229 D4=FNB(D1)*R1/100.
231 P1=P1*A/(A+1)
232 V1=.5*(1-D1/R(1))*FND(D3)*P1
235 V2=.5*(1-D1/R(2))*FNC(D4)*P1*.7
236 IF D1<R(2) THEN 239
237 V2=0
239 V9=V9+(V1+V2)/1.7
240 V3=.5*(1-D1/R(2))*FNC(D4)*P2*.7
241 IF D1<R(2) THEN 245
242 V3=0.
245 V4=.5*(1-D1/R(1))*FND(D3)*P2
246 V8=V8+(V3+V4)/1.7
330 GØ TØ 360
340 D1=D1+D8
350 GØ TØ 365
360 D1=D1+D
365 IF D1>T1 THEN 375
370 GØ TØ 210
375 NEXT K
495 E9=V9/I4
500 S9=V9/V8
505 PRINT "EFFICIENCY=";E9;" SIGNAL/BSLN=";S9
900 DATA 9,89,89,11
905 DATA .95,.95,.50,0.,.08,.08
910 DATA 3.272,1.84E+22,9.22E+22,8.466E-21
915 DATA 7.3,5.5,8735.,5807.
9999 END

```

\*

APPENDIX B: TRIPLE CONVOLUTION OF SOURCE, ABSORBER AND  
 DETECTOR LORENTZIAN PROFILES

```

1 REM CONRES PROGRAM FOR TRIPLE CONVOLUTION OF SOURCE, ABSORBER
2 REM AND DETECTOR LORENTZIAN PROFILES.
10 OPEN 3,OUT PUT,/GRESDT/
12 DIM N(200)
21 READ A(1),P(1),G(1)
22 READ A(2),P(2),G(2)
23 READ A(3),P(3),G(3)
51 DEF FNS(X)=A(1)/(1.+((P(1)-X)/G(1))2)
52 DEF FNA(X)=A(2)/(1.+((P(2)-X)/G(2))2)
53 DEF FND(X)=A(3)/(1.+((P(3)-X)/G(3))2)
80 PRINT "NORMAL HW", "RESONANT HW"
100 FOR Y=1 TO 100
110 LET N(Y)=0.
120 FOR X= - 100 TO 100
130 LET N(Y)=N(Y) + FNS(X)*FNA(X+Y)*FND(X)
150 NEXT X
180 NEXT Y
185 M=0
190 FOR I=1 TO 100
192 IF N(I)<M THEN 200
195 M=N(I)
200 NEXT I
205 FOR I=1 TO 100
210 LET N(I)=N(I)/M
215 WRITE #3,I,N(I)
220 NEXT I
230 I=0
240 I=I+1
250 IF N(I)<.5 THEN 240
260 I1=I-(N(I) - .5)/(N(I)-N(I-1))
270 H=P(2) - I1
280 PRINT 2.*G(2),H
1001 DATA 1.,0.,10.
1002 DATA 1.,50.,10.
1003 DATA 1.,0.,10.

```

\*



**Latest developments in the subject area of this publication, as well as in other areas where the National Bureau of Standards is active, are reported in the NBS Technical News Bulletin. See following page.**

## HOW TO KEEP ABREAST OF NBS ACTIVITIES

Your purchase of this publication indicates an interest in the research, development, technology, or service activities of the National Bureau of Standards.

The best source of current awareness in your specific area, as well as in other NBS programs of possible interest, is the TECHNICAL NEWS BULLETIN, a monthly magazine designed for engineers, chemists, physicists, research and product development managers, librarians, and company executives.

If you do not now receive the TECHNICAL NEWS BULLETIN and would like to subscribe, and/or to review some recent issues, please fill out and return the form below.

|  |
|--|
| <p>Mail to: Office of Technical Information and Publications<br/>National Bureau of Standards<br/>Washington, D. C. 20234</p> <p>Name _____</p> <p>Affiliation _____</p> <p>Address _____</p> <p>City _____ State _____ Zip _____</p> <p><input type="checkbox"/> Please send complimentary past issues of the Technical News Bulletin.</p> <p><input type="checkbox"/> Please enter my 1-yr subscription. Enclosed is my check or money order for \$3.00 (additional \$1.00 for foreign mailing).<br/><i>Check is made payable to: SUPERINTENDENT OF DOCUMENTS.</i></p> <p>TN 541</p> |
|--|

(cut here)

# NBS TECHNICAL PUBLICATIONS

## PERIODICALS

**JOURNAL OF RESEARCH** reports National Bureau of Standards research and development in physics, mathematics, chemistry, and engineering. Comprehensive scientific papers give complete details of the work, including laboratory data, experimental procedures, and theoretical and mathematical analyses. Illustrated with photographs, drawings, and charts.

*Published in three sections, available separately:*

### ● Physics and Chemistry

Papers of interest primarily to scientists working in these fields. This section covers a broad range of physical and chemical research, with major emphasis on standards of physical measurement, fundamental constants, and properties of matter. Issued six times a year. Annual subscription: Domestic, \$9.50; foreign, \$11.75\*.

### ● Mathematical Sciences

Studies and compilations designed mainly for the mathematician and theoretical physicist. Topics in mathematical statistics, theory of experiment design, numerical analysis, theoretical physics and chemistry, logical design and programming of computers and computer systems. Short numerical tables. Issued quarterly. Annual subscription: Domestic, \$5.00; foreign, \$6.25\*.

### ● Engineering and Instrumentation

Reporting results of interest chiefly to the engineer and the applied scientist. This section includes many of the new developments in instrumentation resulting from the Bureau's work in physical measurement, data processing, and development of test methods. It will also cover some of the work in acoustics, applied mechanics, building research, and cryogenic engineering. Issued quarterly. Annual subscription: Domestic, \$5.00; foreign, \$6.25\*.

## TECHNICAL NEWS BULLETIN

The best single source of information concerning the Bureau's research, developmental, cooperative and publication activities, this monthly publication is designed for the industry-oriented individual whose daily work involves intimate contact with science and technology—for *engineers, chemists, physicists, research managers, product-development managers, and company executives*. Annual subscription: Domestic, \$3.00; foreign, \$4.00\*.

\* Difference in price is due to extra cost of foreign mailing.

## NONPERIODICALS

**Applied Mathematics Series.** Mathematical tables, manuals, and studies.

**Building Science Series.** Research results, test methods, and performance criteria of building materials, components, systems, and structures.

**Handbooks.** Recommended codes of engineering and industrial practice (including safety codes) developed in cooperation with interested industries, professional organizations, and regulatory bodies.

**Special Publications.** Proceedings of NBS conferences, bibliographies, annual reports, wall charts, pamphlets, etc.

**Monographs.** Major contributions to the technical literature on various subjects related to the Bureau's scientific and technical activities.

**National Standard Reference Data Series.** NSRDS provides quantitative data on the physical and chemical properties of materials, compiled from the world's literature and critically evaluated.

**Product Standards.** Provide requirements for sizes, types, quality and methods for testing various industrial products. These standards are developed cooperatively with interested Government and industry groups and provide the basis for common understanding of product characteristics for both buyers and sellers. Their use is voluntary.

**Technical Notes.** This series consists of communications and reports (covering both other agency and NBS-sponsored work) of limited or transitory interest.

**Federal Information Processing Standards Publications.** This series is the official publication within the Federal Government for information on standards adopted and promulgated under the Public Law 89-306, and Bureau of the Budget Circular A-86 entitled, Standardization of Data Elements and Codes in Data Systems.

Order NBS publications from:

Superintendent of Documents  
Government Printing Office  
Washington, D.C. 20402

**U.S. DEPARTMENT OF COMMERCE**  
**WASHINGTON, D.C. 20230**

**OFFICIAL BUSINESS**

PENALTY FOR PRIVATE USE, \$300

---



**POSTAGE AND FEES PAID**  
**U.S. DEPARTMENT OF COMMERCE**